Bioorganic & Medicinal Chemistry Letters 20 (2010) 5743–5748

Contents lists available at ScienceDirect

Bioorganic & Medicinal Chemistry Letters

journal homepage: www.elsevier.com/locate/bmcl

^{99m}Tc/Re complexes based on flavone and aurone as SPECT probes for imaging cerebral β-amyloid plaques

Masahiro Ono [a,b,*], Ryoichi Ikeoka [a], Hiroyuki Watanabe [a], Hiroyuki Kimura [b], Takeshi Fuchigami [a], Mamoru Haratake [a], Hideo Saji [b], Morio Nakayama [a,*]

[a] Graduate School of Biomedical Sciences, Nagasaki University, 1-14 Bunkyo-machi, Nagasaki 852-8521, Japan
[b] Graduate School of Pharmaceutical Sciences, Kyoto University, 46-29 Yoshida Shimoadachi-cho, Sakyo-ku, Kyoto 606-8501, Japan

ARTICLE INFO

Article history:
Received 30 June 2010
Revised 28 July 2010
Accepted 2 August 2010
Available online 6 August 2010

Keywords:
Alzheimer's disease
β-Amyloid plaque
Single photon emission computed tomography (SPECT)
Imaging

ABSTRACT

Two ^{99m}Tc/Re complexes based on flavone and aurone were tested as potential probes for imaging β-amyloid plaques using single photon emission computed tomography. Both ^{99m}Tc-labeled derivatives showed higher affinity for Aβ(1–42) aggregates than did ^{99m}Tc-BAT. In sections of brain tissue from an animal model of AD, the Re-flavone derivative **9** and Re-aurone derivative **19** intensely stained β-amyloid plaques. In biodistribution experiments using normal mice, ^{99m}Tc-labeled flavone and aurone displayed similar radioactivity pharmacokinetics. With additional modifications to improve their brain uptake, ^{99m}Tc complexes based on the flavone or aurone scaffold may serve as probes for imaging cerebral β-amyloid plaques.

Alzheimer's disease (AD) is a neurodegenerative disorder of the brain associated with irreversible cognititive decline, memory impairment, and behavioral changes. Currently, the only definitive confirmation of AD is by postmortem histopathological examination of β-amyloid plaques in the brain. The early appraisal of clinical symptoms for a diagnosis of AD is often difficult and unreliable. Numerous reports suggest the accelerated accumulation of β-amyloid plaques in the brain to be a key risk factor associated with AD. Consequently, the detection of individual β-amyloid plaques in vivo by single photon emission computed tomography (SPECT) or positron emission tomography (PET) should improve the diagnosis of and also accelerate the discovery of effective therapeutic agents for AD.[1–4] Many PET/SPECT probes for imaging β-amyloid based on Congo Red, thioflavin T, and DDNP have been reported. Among them, [^{11}C]PIB,[5,6] [^{11}C]SB-13,[7,8] [^{18}F]BAY94-9172,[9,10] [^{11}C]BF-227,[11] [^{18}F]FDDNP,[12,13] [^{123}I]IMPY,[14–16] and [^{18}F]AV-45[17,18] have been tested clinically and demonstrated potential utility. There are more SPECT scanners than PET imaging devices installed for routine clinical imaging, which provides a certain advantage to using SPECT imaging agents. Since SPECT is more valuable than PET in terms of routine diagnostic use, the development of more useful Aβ imaging agents for SPECT has been a critical issue. Although many radioiodinated SPECT imaging agents for detecting β-amyloid plaques have been reported, there are few reports on the development of ^{99m}Tc imaging agents.

^{99m}Tc ($T_{1/2}$ = 6.01 h, 141 keV) has become the most commonly used radionuclide in diagnostic nuclear medicine by SPECT for several reasons: it is readily produced by an ^{99}Mo/^{99m}Tc generator, the gamma-ray energy it emits is suitable for detection, and its physical half-life is compatible with the biological localization and residence time required for imaging. Its ready availability, essentially 24 h a day, and easiness of use make it the radionuclide of choice. New ^{99m}Tc-labeled imaging agents will provide simple, convenient, and widespread SPECT-based imaging methods for detecting and eventually quantifying β-amyloid plaques in living brain tissue.

It has been reported that a dopamine transporter imaging agent, [^{99m}Tc]TRODAT-1, is useful to detect the loss of dopamine neurons in the basal ganglia associated with Parkinson's disease. This is the first example of a ^{99m}Tc imaging agent that can penetrate the blood–brain barrier via a simple diffusion mechanism and localize at sites in the central nervous system. Based on this success, efforts were made to search for comparable ^{99m}Tc imaging agents that target binding sites on β-amyloid plaques in the brain of AD patients. Several ^{99m}Tc-labeled imaging probes have been developed (Fig. 1), but no clinical study of them has been reported.[19–22]

Recently, we have reported that flavonoids including chalcone, flavone, and aurone serve as useful molecular scaffolds in the development of imaging agents for β-amyloid plaques in the brain.[23–28] Initially, we designed and synthesized four ^{99m}Tc-labeled chalcone derivatives with monoamine-monoamide

* Corresponding authors.
E-mail address: ono@pharm.kyoto-u.ac.jp (M. Ono).

0960-894X/$ - see front matter © 2010 Elsevier Ltd. All rights reserved.
doi:10.1016/j.bmcl.2010.08.004

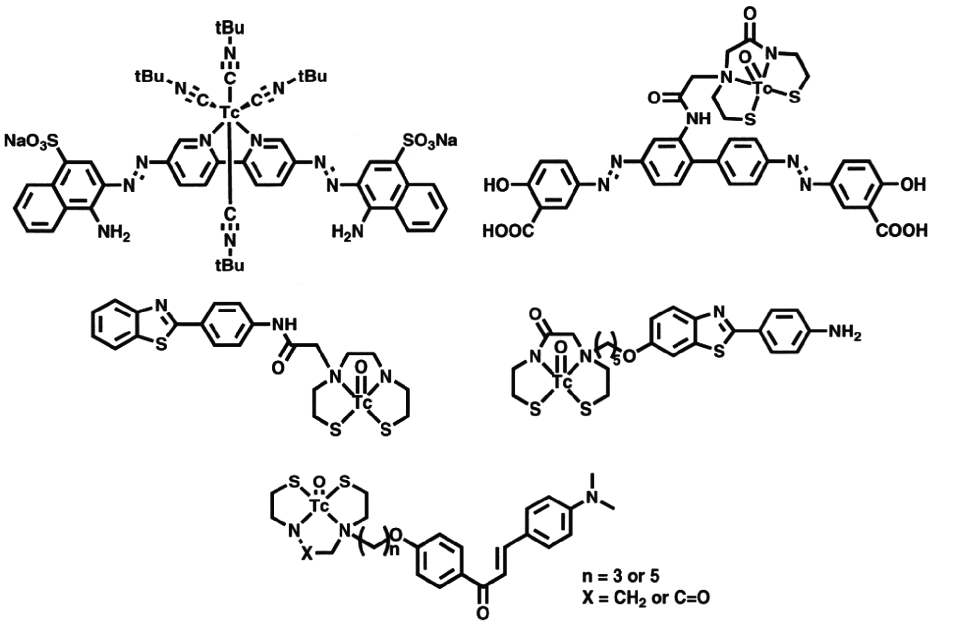

Figure 1. Chemical structure of ^{99m}Tc-labeled Aβ imaging probes reported previously.

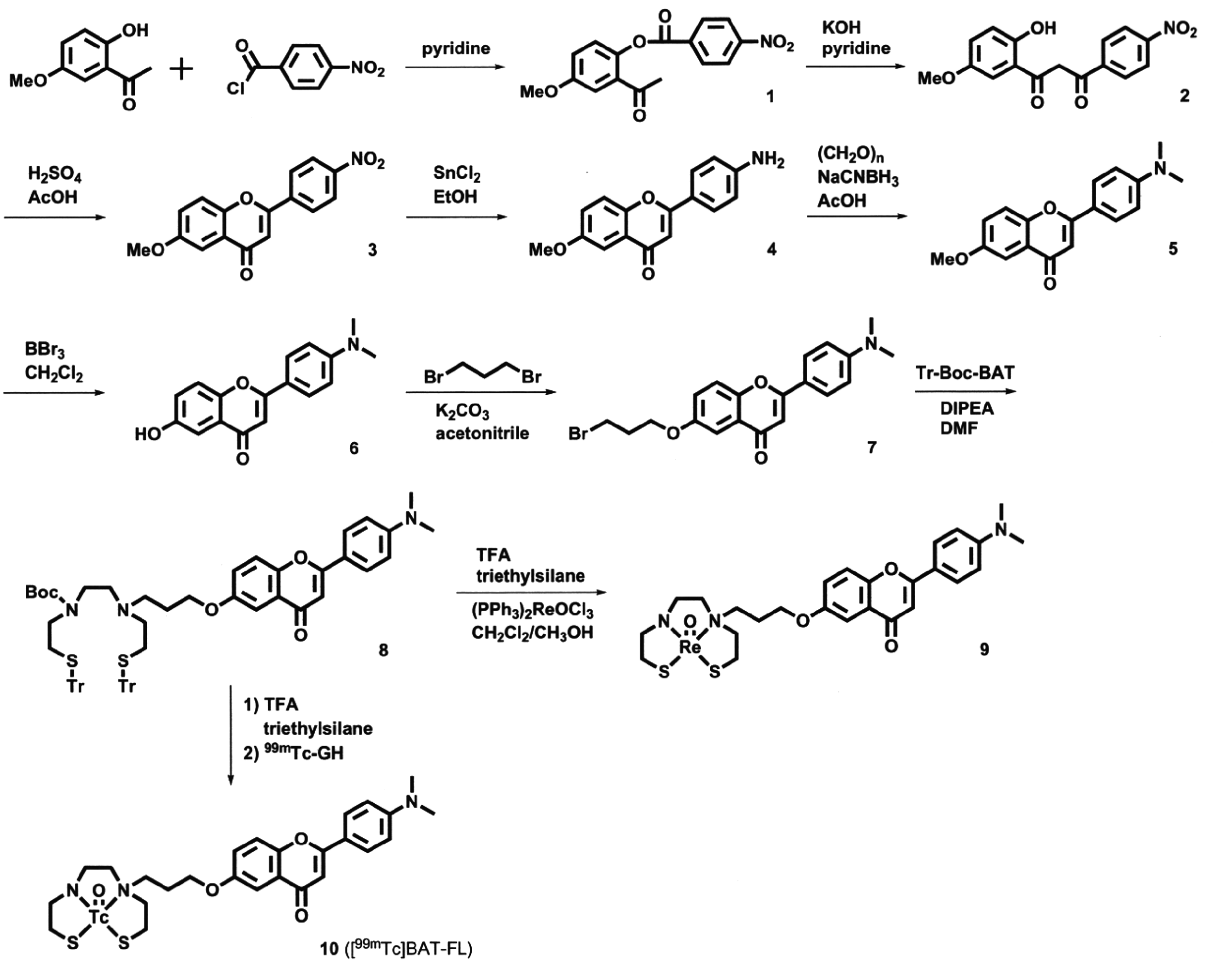

Scheme 1. Synthesis of flavone derivatives.

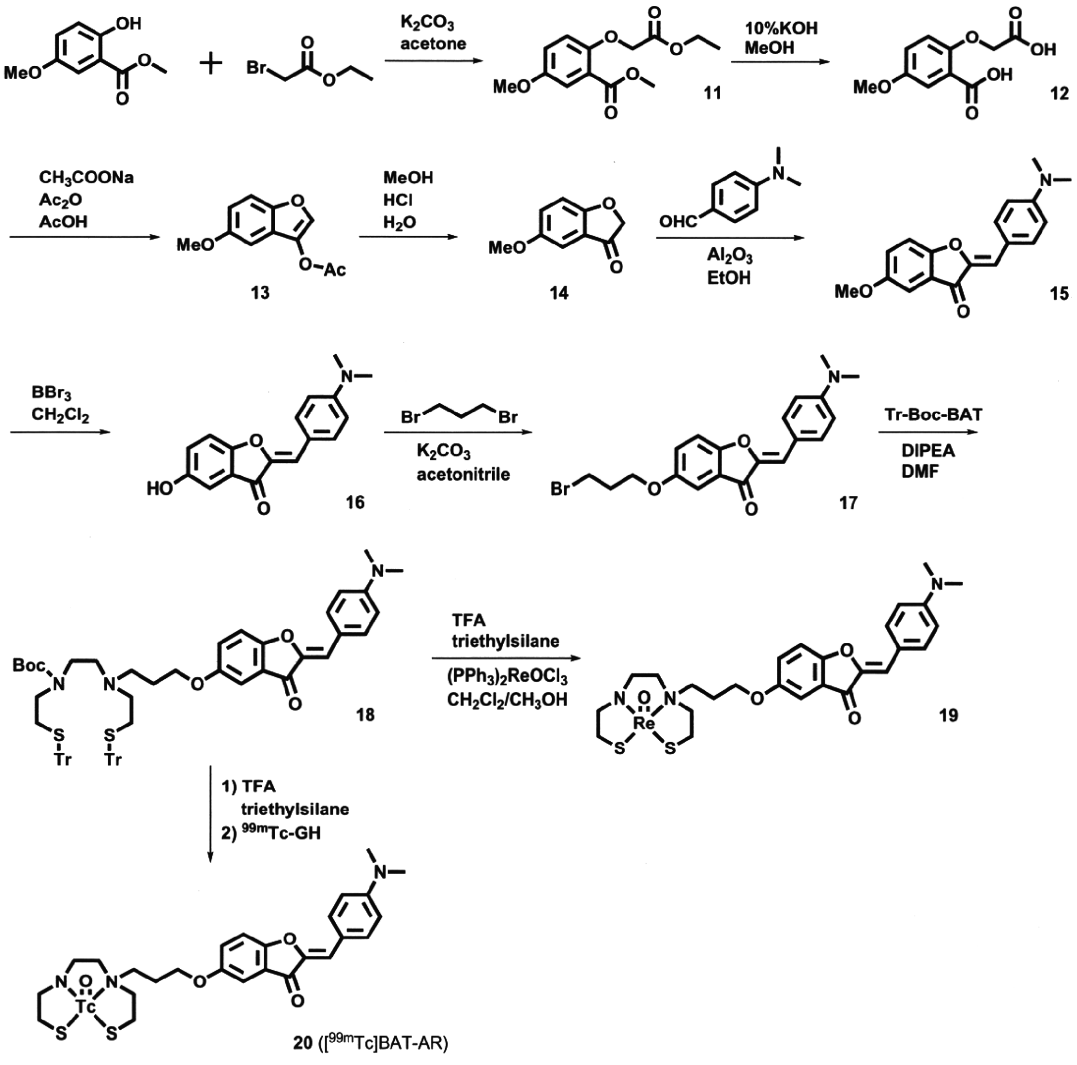

Scheme 2. Synthesis of aurone derivatives.

dithiol (MAMA) and bis-amino-bis-thiol (BAT) (Fig. 1).[29] MAMA and BAT were selected as a chelation ligand taking into consideration the permeability of the blood–brain barrier, because they form an electrically neutral complex with ^{99m}Tc.[30] ^{99m}Tc-BAT-chalcone ($n = 3$) (Fig. 1) showed good uptake into and rapid clearance from the brain in addition to high affinity for β-amyloid plaques, indicating it may be a promising probe for the detection of β-amyloid plaques in the brain.[29] Based on the positive results, we decided to further develop new ^{99m}Tc imaging agents based on the flavonoid scaffold.

In the present study, to develop more useful ^{99m}Tc imaging agents for the clinical diagnosis of AD, we synthesized two flavone and aurone derivatives with BAT as a chelation ligand. We then evaluated the biological potential of these compounds as probes by testing their affinity for Aβ aggregates and β-amyloid plaques in sections of brain tissue from Tg2576 mice and their uptake by and clearance from the brain in biodistribution experiments using normal mice. Also, we compared their usefulness as Aβ imaging probes with a ^{99m}Tc-labeled chalcone derivative reported previously.[29] To our knowledge, this is the first time ^{99m}Tc/Re complexes based on flavone and aurone scaffolds have been proposed as probes for the detection of β-amyloid plaques in the brain.

The synthesis of the ^{99m}Tc/Re complexes based on flavone and aurone was outlined in Schemes 1 and 2. The chelation ligand (BAT) was synthesized according to methods reported previously with some slight modifications.[30] The most useful method of preparing flavones is known as the Baker–Venkataraman transformation.[23] A hydroxyacetophenone was first converted into a benzoyl ester (**1**) which was then treated with a base, forming a 1,3-diketone (**2**). Treatment of this diketone with acid led to the generation of the desired flavone (**3**). The free amino derivative **4** was readily prepared from **3** by reduction with $SnCl_2$ (92% yield). Conversion of **4** to the dimethylamino derivative **5** was achieved by a method reported previously (83% yield). Compound **5** was converted to **6** by demethylation with BBr_3 in CH_2Cl_2 (40% yield). The reaction of dibromopentane with **6** produced the flavone derivative **7** with a trimethine group. Then, **7** was joined to Tr-Boc-BAT to generate **8** (the precursor of ^{99m}Tc/Re reaction). The target aurone derivatives were prepared as shown in Scheme 2. The synthesis of the aurone backbone was achieved via an Aldol reaction of benzofuranones with benzaldehydes using Al_2O_3. 5-Methozy-3-benzofuranone (**14**) was reacted with 4-dimethybenzaldehyde in the presence of Al_2O_3 in chloroform at room temperature to form **15** in a yield of 92%. The precursor of the reaction with ^{99m}Tc/Re, **18**, was obtained

Table 1
HPLC retention times of ^{99m}Tc/Re compounds and log *P* of ^{99m}Tc compounds

Re compounds	Retention time[a] (min)	^{99m}Tc compounds	Retention time[a] (min)	Log *P* of ^{99m}Tc compounds[b]
9	9.5	**10**	11.1	2.77 ± 0.04
19	14.6	**20**	16.6	2.23 ± 0.04

[a] Reversed-phase HPLC using a mixture of H_2O–acetonitrile (2:3) as a mobile phase.
[b] The measurement was done in triplicate and repeated three times. Each value represents the mean ± SD for three independent experiments.

as described for the synthesis of the flavone derivative **8**. After deprotection of the thiol groups in **8** and **18** in TFA and triethylsilane, the Re complexes (**9** and **19**) were prepared through a reaction with $(PPh_3)_2ReOCl_3$. The corresponding ^{99m}Tc complexes, **10** ([^{99m}Tc]BAT-FL) and **20** ([^{99m}Tc]BAT-AR), were prepared by a ligand exchange reaction employing the precursor ^{99m}Tc-glucoheptonate (GH). The resulting mixture was analyzed by reversed-phase HPLC, showing that a single radioactive complex formed with radiochemical purity higher than 95% after purification by HPLC. The identity of the complex was established by comparative HPLC using the corresponding Re complexes as a reference (Table 1). The retention times for [^{99m}Tc]BAT-FL and [^{99m}Tc]BAT-AR on HPLC (radioactivity) were 11.1 and 16.6 min, respectively. The retention times of the corresponding Re complexes on HPLC (UV detection) were 9.5 and 14.6 min, respectively.

In vitro binding experiments to evaluate the affinity of [^{99m}Tc]BAT-FL and [^{99m}Tc]BAT-AR for Aβ(1–42) aggregates were carried out in solutions. The percent radioactivity of [^{99m}Tc]BAT-FL and [^{99m}Tc]BAT-AR bound to aggregates increased dependent on the dose of Aβ(1–42), while [^{99m}Tc]BAT showed no marked affinity for the aggregates (Fig. 2). At all concentrations of Aβ aggregates, [^{99m}Tc]BAT-AR showed significantly greater affinity than [^{99m}Tc]BAT-FL. In these binding experiments, the non-specific binding of [^{99m}Tc]BAT-FL and [^{99m}Tc]BAT-AR was estimated at 1.62–1.85%. The affinity of [^{99m}Tc]BAT-FL and [^{99m}Tc]BAT-AR was less than that of ^{99m}Tc-labeled chalcone derivatives reported previously (Fig. 1).[29] The order in terms of strength of binding corresponded with that of radioiodinated flavonoids,[23–25] indicating that the scaffolds of the [^{99m}Tc]BAT complexes did not play an important role in the affinity for Aβ aggregates.

To confirm the affinity for β-amyloid plaques in the mouse brain, neuropathological fluorescent staining with Re derivatives (**9** and **19**) was carried out using Tg2576 mouse brain sections (Fig. 3). Many β-amyloid plaques were clearly stained with the derivatives (Fig. 3A and B), as reflected by the high affinity for Aβ aggregates in binding assays in vitro. The labeling pattern was consistent with that observed with thioflavin S (Fig.3C and D). These results suggest that [^{99m}Tc]BAT-FL and [^{99m}Tc]BAT-AR would bind to β-amyloid plaques in the mouse brain in addition to having affinity for synthetic Aβ(1–42) aggregates. Although [^{99m}Tc]BAT-AR showed greater affinity than [^{99m}Tc]BAT-AR in the binding assays in vitro, no marked difference in binding between [^{99m}Tc]BAT-FL and [^{99m}Tc]BAT-AR was observed in the fluorescent staining experiments.

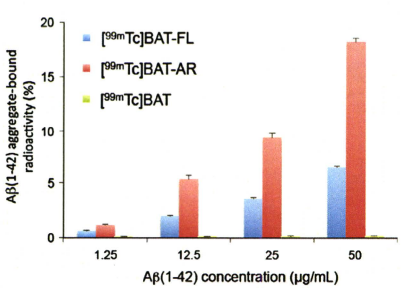

Figure 2. Binding assay of [^{99m}Tc]BAT-FL, [^{99m}Tc]BAT-AR, and [^{99m}Tc]BAT with Aβ(1–42) aggregates. Values are the mean ± standard error of the mean for three independent experiments.

[^{99m}Tc]BAT-FL and [^{99m}Tc]BAT-AR were examined as to their biodistribution in normal mice (Table 2). A biodistribution study provides important information on brain uptake. The ideal probe for imaging β-amyloid should penetrate the blood–brain barrier well enough to deliver a sufficient dose into the brain while clearing rapidly from normal regions so as to achieve a high signal to noise ratio in the AD brain. Previous studies suggest that the optimal lipophilicity for entry into the brain is obtained with log *P* values of between 1 and 3. [^{99m}Tc]BAT-FL and [^{99m}Tc]BAT-AR had log *P* values of 2.77 and 2.23, respectively (Table 1), but showed less uptake, 0.64 and 0.79%ID/g at 2 min postinjection, than expected. Thereafter, the radioactivity of [^{99m}Tc]BAT-FL and [^{99m}Tc]BAT-AR that accumulated in the brain was rapidly eliminated (0.23 and 0.11%ID/g at 60 min postinjection). Recently, we have reported that the ^{99m}Tc-labeled chalcone derivative showed high uptake (1.48%ID/g at 2 min postinjection) into and rapid clearance (0.17%ID/g at 60 min postinjection) from the brain, a highly desirable property for imaging agents for β-amyloid plaques.[29] The pharmacokinetics of the ^{99m}Tc-labeled chalcone derivative in the brain appears superior to that of any ^{99m}Tc-labeled probes reported previously, indicating that this compound should be investigated further as a potentially useful probe for imaging β-amyloid. Compared with that of the ^{99m}Tc-labeled chalcone,[29] the radioactivity of [^{99m}Tc]BAT-FL and [^{99m}Tc]BAT-AR appears insufficient for the imaging of β-amyloid plaques in the brain. Since the affinity of [^{99m}Tc]BAT-FL and [^{99m}Tc]BAT-AR for Aβ aggregates was as high as that of ^{99m}Tc-labeled chalcone derivatives,[29] improvement of the uptake of [^{99m}Tc]BAT-FL and [^{99m}Tc]BAT-AR is an important prerequisite to developing more useful ^{99m}Tc-labeled probes. Therefore, additional structural changes in the flavone and aurone scaffold are needed to further improve the pharmacokinetics of [^{99m}Tc]BAT-FL and [^{99m}Tc]BAT-AR in vivo.

In conclusion, we successfully designed and synthesized novel ^{99m}Tc/Re complexes based on flavone and aurone for the detection of β-amyloid plaques in the brain. Both [^{99m}Tc]BAT-FL and [^{99m}Tc]BAT-AR showed high affinity for synthetic Aβ(1–42) aggregates. In experiments in vitro using sections of brain from Tg2576 mice, Re complexes intensely stained β-amyloid plaques. In addition, [^{99m}Tc]BAT-FL and [^{99m}Tc]BAT-AR displayed good uptake into and a rapid washout from the brain after their injection in normal mice. This combination of affinity for β-amyloid plaques, and good uptake and clearance makes [^{99m}Tc]BAT-FL and [^{99m}Tc]BAT-AR promising probes for the detection of β-amyloid plaques in the brain, although additional modifications are required to enhance their uptake. The results of the present study should provide information useful for the development of ^{99m}Tc-labeled probes for the imaging of β-amyloid plaques in the brain.

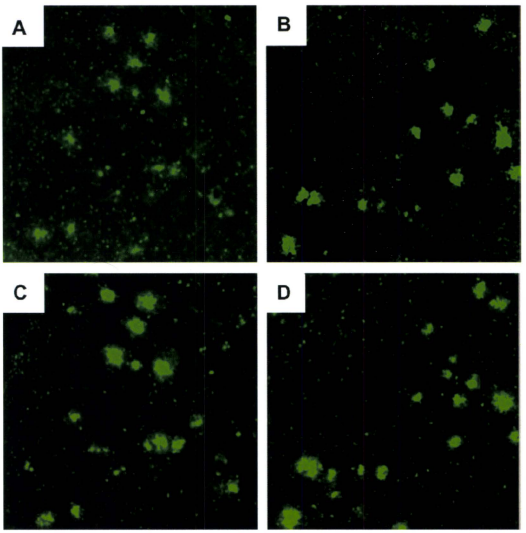

Figure 3. Fluorescent staining of the flavone derivative **9** (A), and aurone derivative **19** (B) in Tg2576 mouse brain. Labeled plaques were confirmed by staining the adjacent sections with thioflavin S (C and D).

Table 2
Biodistribution of radioactivity after injection of [^{99m}Tc]BAT-FL and [^{99m}Tc]BAT-AR in normal mice[a]

Organ	Time after injection (min)			
	2	10	30	60
[^{99m}Tc]*BAT-FL* (**10**)				
Blood	1.90 (0.08)	0.80 (0.16)	0.41 (0.06)	0.28 (0.06)
Liver	19.35 (1.30)	24.75 (3.45)	27.73 (3.30)	24.12 (3.08)
Kidney	9.70 (0.83)	5.56 (0.84)	2.38 (0.30)	1.40 (0.20)
Intestine[b]	4.54 (0.42)	11.36 (1.88)	26.61 (3.93)	42.67 (2.98)
Spleen	3.24 (0.61)	2.21 (0.31)	1.04 (0.42)	0.45 (0.07)
Lung	11.42 (2.10)	3.84 (0.57)	1.70 (0.24)	1.07 (0.16)
Stomach[b]	0.90 (0.15)	1.36 (0.55)	1.52 (0.67)	2.45 (1.04)
Pancreas	4.41 (0.29)	4.31 (0.35)	1.89 (0.15)	0.84 (0.17)
Heart	12.00 (1.16)	3.12 (0.51)	0.99 (0.18)	0.44 (0.09)
Brain	0.64 (0.07)	0.57 (0.14)	0.36 (0.01)	0.23 (0.04)
[^{99m}Tc]*BAT-AR* (**20**)				
Blood	1.56 (0.16)	0.71 (0.07)	0.35 (0.04)	0.21 (0.04)
Liver	17.76 (1.51)	17.77 (1.70)	15.17 (0.95)	12.96 (1.48)
Kidney	11.50 (0.73)	8.77 (1.15)	4.83 (0.77)	3.28 (1.52)
Intestine[b]	6.78 (0.78)	26.20 (2.45)	46.06 (3.17)	55.33 (7.42)
Spleen	2.87 (0.30)	1.92 (0.47)	0.70 (0.07)	0.35 (0.15)
Lung	6.10 (1.15)	3.25 (0.78)	1.63 (0.42)	0.85 (0.18)
Stomach[b]	1.03 (0.13)	1.63 (0.25)	1.88 (0.11)	1.69 (0.49)
Pancreas	5.85 (1.09)	4.20 (0.68)	1.53 (0.54)	0.60 (0.30)
Heart	12.30 (1.21)	3.26 (0.43)	1.15 (0.30)	0.40 (0.09)
Brain	0.79 (0.12)	0.70 (0.05)	0.27 (0.06)	0.11 (0.04)

[a] Each value represents the mean (SD) for 3–6 mice at each interval. Expressed as % injected dose per gram.
[b] Expressed as % injected dose per organ.

Acknowledgments

This study was supported by the Program for Promotion of Fundamental Studies in Health Sciences of the National Institute of Biomedical Innovation (NIBIO), a Health Labour Sciences Research Grant, and a Grant-in-aid for Young Scientists (A) and Exploratory Research from the Ministry of Education, Culture, Sports, Science and Technology, Japan.

Supplementary data

Supplementary data (procedure for the preparation of ^{99m}Tc/Re complexes, in vitro binding assay, in vitro fluorescent staining using Tg2576 mouse brain sections, and biodistribution experiments) associated with this article can be found, in the online version, at doi:10.1016/j.bmcl.2010.08.004.

References and notes

1. Selkoe, D. J. *Physiol. Rev.* **2001**, *81*, 741.
2. Selkoe, D. J. *Nat. Biotechnol.* **2000**, *18*, 823.
3. Mathis, C. A.; Wang, Y.; Klunk, W. E. *Curr. Pharm. Des.* **2004**, *10*, 1469.
4. Nordberg, A. *Lancet Neurol.* **2004**, *3*, 519.
5. Mathis, C. A.; Wang, Y.; Holt, D. P.; Huang, G. F.; Debnath, M. L.; Klunk, W. E. *J. Med. Chem.* **2003**, *46*, 2740.
6. Klunk, W. E.; Engler, H.; Nordberg, A.; Wang, Y.; Blomqvist, G.; Holt, D. P.; Bergstrom, M.; Savitcheva, I.; Huang, G. F.; Estrada, S.; Ausen, B.; Debnath, M. L.; Barletta, J.; Price, J. C.; Sandell, J.; Lopresti, B. J.; Wall, A.; Koivisto, P.; Antoni, G.; Mathis, C. A.; Langstrom, B. *Ann. Neurol.* **2004**, *55*, 306.
7. Ono, M.; Wilson, A.; Nobrega, J.; Westaway, D.; Verhoeff, P.; Zhuang, Z. P.; Kung, M. P.; Kung, H. F. *Nucl. Med. Biol.* **2003**, *30*, 565.
8. Verhoeff, N. P.; Wilson, A. A.; Takeshita, S.; Trop, L.; Hussey, D.; Singh, K.; Kung, H. F.; Kung, M. P.; Houle, S. *Am. J. Geriatr. Psychiatry* **2004**, *12*, 584.
9. Zhang, W.; Oya, S.; Kung, M. P.; Hou, C.; Maier, D. L.; Kung, H. F. *Nucl. Med. Biol.* **2005**, *32*, 799.
10. Rowe, C. C.; Ackerman, U.; Browne, W.; Mulligan, R.; Pike, K. L.; O'Keefe, G.; Tochon-Danguy, H.; Chan, G.; Berlangieri, S. U.; Jones, G.; Dickinson-Rowe, K. L.; Kung, H. P.; Zhang, W.; Kung, M. P.; Skovronsky, D.; Dyrks, T.; Holl, G.; Krause, S.; Friebe, M.; Lehman, L.; Lindemann, S.; Dinkelborg, L. M.; Masters, C. L.; Villemagne, V. L. *Lancet Neurol.* **2008**, *7*, 129.

11. Kudo, Y.; Okamura, N.; Furumoto, S.; Tashiro, M.; Furukawa, K.; Maruyama, M.; Itoh, M.; Iwata, R.; Yanai, K.; Arai, H. *J. Nucl. Med.* **2007**, *48*, 553.
12. Agdeppa, E. D.; Kepe, V.; Liu, J.; Flores-Torres, S.; Satyamurthy, N.; Petric, A.; Cole, G. M.; Small, G. W.; Huang, S. C.; Barrio, J. R. *J. Neurosci.* **2001**, *21*, RC189.
13. Shoghi-Jadid, K.; Small, G. W.; Agdeppa, E. D.; Kepe, V.; Ercoli, L. M.; Siddarth, P.; Read, S.; Satyamurthy, N.; Petric, A.; Huang, S. C.; Barrio, J. R. *Am. J. Geriatr. Psychiatry* **2002**, *10*, 24.
14. Kung, M. P.; Hou, C.; Zhuang, Z. P.; Zhang, B.; Skovronsky, D.; Trojanowski, J. Q.; Lee, V. M.; Kung, H. F. *Brain Res.* **2002**, *956*, 202.
15. Zhuang, Z. P.; Kung, M. P.; Wilson, A.; Lee, C. W.; Plossl, K.; Hou, C.; Holtzman, D. M.; Kung, H. F. *J. Med. Chem.* **2003**, *46*, 237.
16. Newberg, A. B.; Wintering, N. A.; Clark, C. M.; Plossl, K.; Skovronsky, D.; Seibyl, J. P.; Kung, M. P.; Kung, H. F. *J. Nucl. Med.* **2006**, *47*, 78P.
17. Zhang, W.; Kung, M. P.; Oya, S.; Hou, C.; Kung, H. F. *Nucl. Med. Biol.* **2007**, *34*, 89.
18. Choi, S. R.; Golding, G.; Zhuang, Z.; Zhang, W.; Lim, N.; Hefti, F.; Benedum, T. E.; Kilbourn, M. R.; Skovronsky, D.; Kung, H. F. *J. Nucl. Med.* **2009**, *50*, 1887.
19. Han, H.; Cho, C. G.; Lansbury, P. T., Jr. *J. Am. Chem. Soc.* **1996**, *118*, 4506.
20. Dezutter, N. A.; Dom, R. J.; de Groot, T. J.; Bormans, G. M.; Verbruggen, A. M. *Eur. J. Nucl. Med.* **1999**, *26*, 1392.
21. Chen, X.; Yu, P.; Zhang, L.; Liu, B. *Bioorg. Med. Chem. Lett.* **2008**, *18*, 1442.
22. Serdons, K.; Verduyckt, T.; Cleynhens, J.; Terwinghe, C.; Mortelmans, L.; Bormans, G.; Verbruggen, A. *Bioorg. Med. Chem. Lett.* **2007**, *17*, 6086.
23. Ono, M.; Yoshida, N.; Ishibashi, K.; Haratake, M.; Arano, Y.; Mori, H.; Nakayama, M. *J. Med. Chem.* **2005**, *48*, 7253.
24. Ono, M.; Haratake, M.; Mori, H.; Nakayama, M. *Bioorg. Med. Chem.* **2007**, *15*, 6802.
25. Ono, M.; Maya, Y.; Haratake, M.; Ito, K.; Mori, H.; Nakayama, M. *Biochem. Biophys. Res. Commun.* **2007**, *361*, 116.
26. Maya, Y.; Ono, M.; Watanabe, H.; Haratake, M.; Saji, H.; Nakayama, M. *Bioconjugate Chem.* **2009**, *20*, 95.
27. Ono, M.; Watanabe, R.; Kawashima, H.; Cheng, Y.; Kimura, H.; Watanabe, H.; Haratake, M.; Saji, H.; Nakayama, M. *J. Med. Chem.* **2009**, *52*, 6394.
28. Ono, M.; Watanabe, R.; Kawashima, H.; Kawai, T.; Watanabe, H.; Haratake, M.; Saji, H.; Nakayama, M. *Bioorg. Med. Chem.* **2009**, *17*, 2069.
29. Ono, M.; Ikeoka, R.; Watanabe, H.; Fuchigami, T.; Haratake, M.; Saji, H.; Nakayama, M. *ACS Chem. Neurosci.*, in press, doi:10.1021/cn100042d.
30. Oya, S.; Plossl, K.; Kung, M. P.; Stevenson, D. A.; Kung, H. F. *Nucl. Med. Biol.* **1998**, *25*, 135.

ACS Medicinal Chemistry Letters

pubs.acs.org/acsmedchemlett

Novel Benzofurans with ^{99m}Tc Complexes as Probes for Imaging Cerebral β-Amyloid Plaques

Masahiro Ono,*[,†,‡] Yasufumi Fuchi,[†] Takeshi Fuchigami,[†] Nobuya Kobashi,[†] Hiroyuki Kimura,[‡] Mamoru Haratake,[†] Hideo Saji,[‡] and Morio Nakayama*[,†]

[†]Graduate School of Biomedical Sciences, Nagasaki University, 1-14 Bunkyo-machi, Nagasaki 852-8521, Japan, and [‡]Graduate School of Pharmaceutical Sciences, Kyoto University, 46-29 Yoshida Shimoadachi-cho, Sakyo-ku, Kyoto 606-8501, Japan

ABSTRACT Two novel benzofuran derivatives coupled with ^{99m}Tc complexes were tested as probes for imaging cerebral β-amyloid plaques using single photon emission tomography. Although both derivatives bound to Aβ(1−42) aggregates, ^{99m}Tc-BAT-BF showed higher affinity than ^{99m}Tc-MAMA-BF. In sections of brain tissue from an animal model of AD, ^{99m}Tc-BAT-BF clearly labeled β-amyloid plaques. In biodistribution experiments using normal mice, ^{99m}Tc-BAT-BF displayed high uptake soon after its injection and washed out from the brain rapidly, a highly desirable feature for an imaging agent. ^{99m}Tc-BAT-BF may be a potential probe for imaging β-amyloid plaques in Alzheimer's brains.

KEYWORDS Alzheimer's disease, β-amyloid plaque, Tc-99m, single photon emission computed tomography (SPECT), imaging

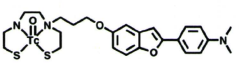

8 (^{99m}Tc-BAT-BF)

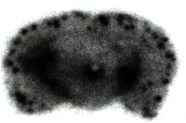

Alzheimer's disease (AD) is a neurodegenerative disease of the brain associated with irreversible cognitive decline, memory impairment, and behavioral changes. The presence of β-amyloid (Aβ) aggregates in the brain is generally accepted as a hallmark of AD.[1,2] Currently, the only definitive diagnosis of AD is by pathological examination of the postmortem staining of affected brain tissue, and the early appraisal of clinical symptoms for the diagnosis of AD is often difficult and unreliable. Thus, the detection of individual plaques in vivo by single photon emission tomography (SPECT) or positron emission tomography (PET) has been strongly desired to improve diagnosis and also accelerate the discovery of effective therapeutic agents for AD.[3−6] Many radiolabeled probes for imaging β-amyloid based on Congo Red, thioflavin T, and DDNP have been reported. Among them, [^{11}C]PIB,[7,8] [^{11}C]SB-13,[9,10] [^{18}F]BAY94-9172,[11,12] [^{11}C]BF-227,[13] [^{18}F]FDDNP,[14−16] [^{123}I]IMPY,[17−19] and [^{18}F]AV-45[20,21] have been tested clinically and demonstrated potential utility.

We have recently reported that ^{125}I-, ^{11}C-, and ^{18}F-labeled benzofuran derivatives showed high affinity for Aβ aggregates and good uptake into and rapid clearance from the brain, indicating that benzofuran can function as a promising scaffold for the development of β-amyloid imaging probes.[22,23] In this study, we planned the development of novel benzofuran derivatives labeled with technetium-99 m (^{99m}Tc). ^{99m}Tc ($T_{1/2}$ = 6.01 h, 141 keV) has become the most commonly used radionuclide in diagnostic nuclear medicine, because it is readily produced by an ^{99}Mo/^{99m}Tc generator; the medium γ-ray energy that it emits is suitable for detection, and its physical half-life is compatible with the biological localization and residence time required for imaging. Its ready availability, essentially 24 h a day, and easiness of use make it the radionuclide of choice. Several ^{99m}Tc-labeled imaging probes have been developed (Figure 1),[24−28] but no clinical study of them has been reported. New ^{99m}Tc-labeled imaging agents will provide simple, convenient, and widespread SPECT-based imaging methods for detecting and eventually quantifying β-amyloid plaques in living brain tissue.

In the present study, we synthesized two benzofuran derivatives with monoamine-monoamide dithiol (MAMA) and bis-amino-bis-thiol (BAT). MAMA and BAT were selected as a chelation ligand taking into consideration the permeability of the blood−brain barrier, because they form an electrically neutral complex with ^{99m}Tc.[29] We then evaluated their biological potential as probes by testing their affinity for Aβ aggregates and β-amyloid plaques in sections of brain tissue from Tg2576 mice and their uptake by and clearance from the brain in biodistribution experiments using normal mice. To our knowledge, this is the first time that benzofurans coupled with ^{99m}Tc complexes have been proposed as probes for the detection of β-amyloid plaques in the brain.

The synthesis of the ^{99m}Tc/Re benzofuran derivatives is outlined in Scheme 1. The key step in the formation of the benzofuran backbone was readily achieved by reacting 2-hydroxy-5-methoxybenzaldehyde with 4-nitrobenzylbromide to produce compound **1** in a yield of 75%. The amino derivative **2** was prepared from **1** by reduction with $SnCl_2$ in a yield of 95%.

Received Date: June 16, 2010
Accepted Date: July 26, 2010
Published on Web Date: August 02, 2010

ACS Medicinal Chemistry Letters

pubs.acs.org/acsmedchemlett

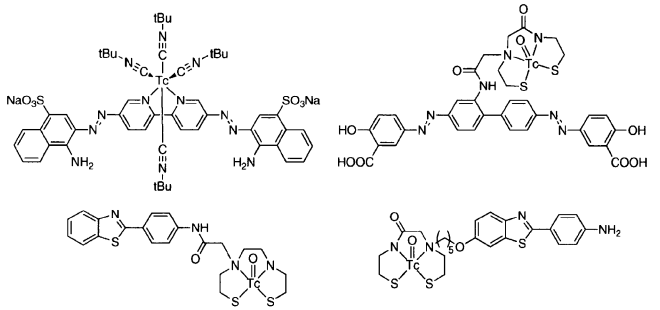

Figure 1. Chemical structure of ^{99m}Tc-labeled Aβ imaging probes reported previously.

Scheme 1. Synthesis of Re- and ^{99m}Tc-benzofuran Derivatives[a]

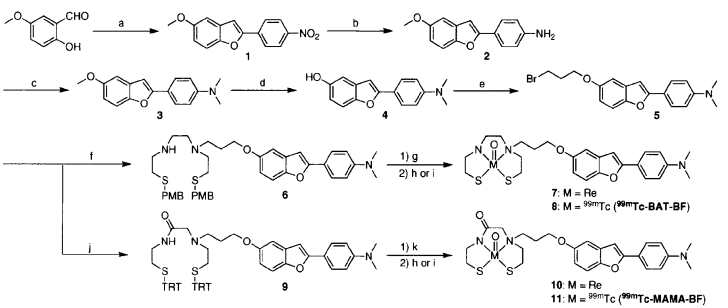

[a] Reagents: (a) DMF, K_2CO_3, 4-nitrobenzylbromide. (b) EtOH, $SnCl_2$. (c) CH_3COOH, $(CH_2O)_n$, $NaBH_3CN$. (d) CH_2Cl_2, BBr_3. (e) CH_3CN, K_2CO_3, 1,3-dibromopropane. (f) CH_3CN, DIPEA, PMB-BAT. (g) TFA, $MeSO_3H$, anisole. (h) CH_2Cl_2/MeOH, $(PPh_3)_2ReOCl_3$, AcONa. (i) CH_3CN, 0.1 N HCl, ^{99m}Tc-GH. (j) CH_3CN, TRT-MAMA, DIPEA. (k) TFA, Et_3SiH.

Conversion of **2** to the dimethylamino derivative **3** was achieved by an efficient method with paraformaldehyde, sodium cyanoborohydride, and acetic acid (78% yield). The *O*-methyl group of **3** was removed by reacting with BBr_3 to give **4** in a yield of 63%. After a trimethylene group was introduced into **4** as a linker by reacting with 1,3-dibromopropane, the chelation ligands were conjugated with **5**. The thiol-protected chelation ligands (PMB-BAT and TRT-MAMA) were synthesized according to methods reported previously with some slight modifications. Then, **5** was joined to PMB-BAT or TRT-MAMA to generate the compounds **6** (PMB-BAT-BF) and **9** (TRT-MAMA-BF), respectively. After deprotection of the thiol group in **6** and **9**, the Re complexes (**7** and **10**) were directly prepared by a reaction with $(PPh_3)_2ReOCl_3$. The corresponding ^{99m}Tc complex, **8** (^{99m}Tc-BAT-BF) or **11** (^{99m}Tc-MAMA-BF), was prepared by a ligand exchange reaction employing the precursor ^{99m}Tc-glucoheptonate (GH). The resulting mixture was analyzed by reversed-phase high-performance liquid chromatography (HPLC), showing that a single radioactive complex formed with radiochemical purity higher than 95% after purification by HPLC. The identity of the complex was established by comparative HPLC using the corresponding Re complexes as a reference. The retention times for ^{99m}Tc-BAT-BF and ^{99m}Tc-MAMA-BF on HPLC (radioactivity) were 13.2 and 10.3 min, respectively. The retention times of the corresponding Re complexes (**7** and **10**) on HPLC (UV detection) were 11.4 and 9.4 min, respectively.

To evaluate the binding affinity of Re-BAT-BF (**7**) and Re-MAMA-BF (**10**), inhibition assays with [^{125}I]IMPY and Aβ(1−42) aggregates were performed (Figure 2).[18] Both ligands inhibited the binding of [^{125}I]IMPY to Aβ(1−42) aggregates in a dose-dependent manner, indicating an affinity for Aβ aggregates. Their K_i values were 11.5 and 24.4 nM, respectively, suggesting that Re-BAT-BF displayed higher affinity than Re-MAMA-BF (Table 1). The results also indicated that ^{99m}Tc-BAT-BF and ^{99m}Tc-MAMA-BF would bind Aβ aggregates. Indeed, in subsequent assays, ^{99m}Tc-BAT-BF and ^{99m}Tc-MAMA-BF showed higher affinity than ^{99m}Tc-BAT and ^{99m}Tc-MAMA (Figure S1 in the Supporting Information). These results

DOI: 10.1021/ml100140d | ACS Med. Chem. Lett. 2010, 1, 443–447

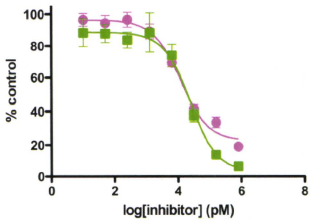

Figure 2. Inhibition curves of Re-BAT-BF (**7**) (pink circle) and Re-MAMA-BF (**10**) (green square) for the binding of [^{125}I]IMPY to Aβ(1−42) aggregates.

Table 1. Inhibition Constants for the Binding of [^{125}I]IMPY to Aβ(1−42) Aggregates

compound	K_i (nM)[a]
Re-BAT-BF (**7**)	11.5 ± 0.56
Re-MAMA-BF (**10**)	24.4 ± 0.77

[a] Values are the means ± standard errors of the mean of three independent determinations.

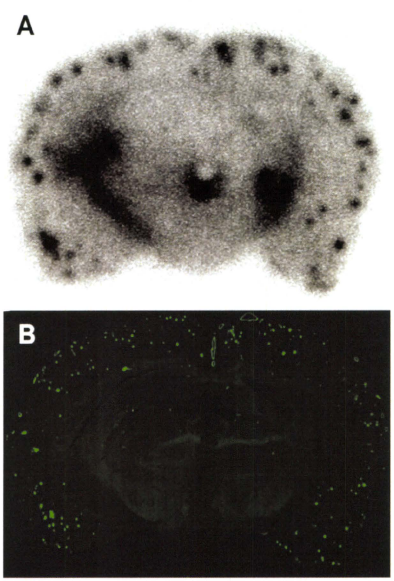

Figure 3. Autoradiography of ^{99m}Tc-BAT-BF in sections from Tg2576 mouse brain (A). Labeled plaques were confirmed by the staining of the adjacent sections with thioflavin-S (B).

strongly support our previous report that benzofuran derivatives have considerable tolerance for structural modifications.[22,23]

Next, the affinity of ^{99m}Tc-BAT-BF for β-amyloid plaques was investigated in vitro using sections of Tg2576 mouse brain (Figure 3). Autoradiographic images showed many radioactive spots in the brain tissue. Furthermore, the radioactivity of ^{99m}Tc-BAT-BF corresponded with the areas of staining with thioflavin-S, a pathological dye commonly used for β-amyloid plaques. In contrast, normal mouse brain displayed no remarkable accumulation of ^{99m}Tc-BAT-BF (data not shown). The results suggest that ^{99m}Tc-BAT-BF binds affinity for β-amyloid plaques in the mouse brain in addition to binding synthetic Aβ aggregates.

The biodistribution of ^{99m}Tc-BAT-BF and ^{99m}Tc-MAMA-BF was examined in normal mice (Table 2). A biodistribution experiment provides important information on uptake in the brain. The ideal imaging probe should penetrate the blood−brain barrier to deliver a sufficient dose into the brain but be rapidly cleared from normal regions so as to achieve in a high signal-to-noise ratio. ^{99m}Tc-BAT-BF showed greater uptake (1.34% ID/g) than ^{99m}Tc-MAMA-BF (0.74% ID/g) at 2 min postinjection. The uptake of ^{99m}Tc-BAT-BF peaked at 10 min postinjection, reaching 1.37% ID/g, and about 60% of radioactivity accumulated at 2 min postinjection had been washed out from the brain by 60 min. The uptake of

Table 2. Biodistribution of Radioactivity after Injection of ^{99m}Tc-Labeled Benzofuran Derivatives in Normal Mice[a]

	time after injection (min)			
organ	2	10	30	60
	^{99m}Tc-BAT-BF (**8**)			
blood	4.40 (0.27)	1.96 (0.06)	1.93 (0.26)	2.15 (0.91)
liver	21.94 (5.94)	20.87 (1.28)	19.65 (1.31)	15.09 (3.83)
kidney	10.28 (1.76)	7.90 (0.40)	4.27 (0.18)	2.70 (0.57)
intestine[b]	1.45 (0.18)	3.68 (0.52)	7.42 (1.62)	9.02 (1.93)
spleen	5.20 (1.01)	3.09 (0.23)	1.69 (0.21)	1.16 (0.14)
lung	26.70 (2.27)	6.48 (1.33)	3.51 (0.64)	2.36 (0.48)
stomach[b]	1.33 (0.57)	1.90 (0.43)	4.09 (1.37)	4.17 (1.92)
pancreas	4.14 (0.77)	4.57 (0.24)	2.98 (0.38)	1.42 (0.15)
heart	17.60 (2.60)	8.29 (0.97)	3.28 (1.35)	1.51 (0.25)
brain	1.34 (0.12)	1.37 (0.18)	0.94 (0.20)	0.56 (0.07)
	^{99m}Tc-MAMA-BF (**11**)			
blood	4.13 (0.42)	1.78 (0.25)	2.15 (0.12)	2.24 (0.24)
liver	20.17 (3.81)	21.62 (2.62)	23.32 (1.59)	20.16 (2.13)
kidney	7.37 (1.06)	8.09 (1.16)	5.11 (0.29)	3.28 (0.45)
intestine[b]	0.95 (0.22)	2.13 (0.19)	4.75 (0.93)	5.73 (0.66)
spleen	4.48 (0.56)	3.69 (0.34)	3.49 (0.61)	2.59 (0.65)
lung	24.04 (5.17)	7.59 (2.13)	4.24 (0.35)	3.54 (1.26)
stomach[b]	0.73 (0.21)	2.35 (0.58)	4.94 (0.57)	2.81 (0.51)
pancreas	2.70 (0.47)	4.00 (1.28)	5.48 (0.61)	3.76 (0.36)
heart	12.28 (2.20)	10.48 (1.79)	5.05 (0.90)	2.16 (0.34)
brain	0.74 (0.15)	0.99 (0.22)	1.23 (0.09)	0.89 (0.08)

[a] Each value represents the mean (SD) for five mice. Expressed as % injected dose per gram. [b] Expressed as % injected dose per organ.

DOI: 10.1021/ml100140d | ACS Med. Chem. Lett. 2010, 1, 443–447

^{99m}Tc-MAMA-BF peaked 30 min after the injection at 1.23% ID/g, and the washout from the brain was slower than that of ^{99m}Tc-BAT-BF throughout the time course, which is unsuitable for imaging in vivo. The log *P* values of ^{99m}Tc-BAT-BF and ^{99m}Tc-MAMA-BF were 3.33 and 3.01, respectively. Although lipophilicity is just one of the factors affecting the uptake of a compound into the brain,[4] it may explain the good uptake of ^{99m}Tc-BAT-BF.

In conclusion, we successfully designed and synthesized novel benzofuran derivatives conjugated with ^{99m}Tc or Re complexes for the detection of β-amyloid plaques in the brain. In experiments in vitro, Re-BAT-BF bound to Aβ aggregates with greater affinity than did Re-MAMA-BF, and ^{99m}Tc-BAT-BF clearly labeled β-amyloid plaques in sections of brain tissue from Tg2576 mice. In addition, ^{99m}Tc-BAT-BF displayed good uptake into and a rapid washout from the brain after its injection in normal mice. The combination of good affinity for β-amyloid plaques, uptake, and clearance makes ^{99m}Tc-BAT-BF a promising probe for the detection of β-amyloid plaques in the brain. The results of the present study should provide useful information for the development of ^{99m}Tc-labeled probes for the imaging of β-amyloid plaques in the brain.

SUPPORTING INFORMATION AVAILABLE Procedures for the preparation of new ligands, analysis of data, experiments in vitro, and biodistribution experiments. This material is available free of charge via the Internet at http://pubs.acs.org.

AUTHOR INFORMATION

Corresponding Author: *To whom correspondence should be addressed. Tel: +81-75-753-4608. Fax: +81-75-753-4568. E-mail: ono@pharm.kyoto-u.ac.jp (M.O.). Tel: +81-95-819-2441. Fax: +81-95-819-2441. E-mail: morio@nagasaki-u.ac.jp (M.N.).

Funding Sources: This study was supported by Grants-in-Aid for Scientific Research (B), Young Scientists (A), and Exploratory Research from the Ministry of Education, Culture, Sports, Science and Technology, Japan.

REFERENCES

(1) Hardy, J. A.; Higgins, G. A. Alzheimer's disease: The amyloid cascade hypothesis. *Science* **1992,** *256*, 184–185.

(2) Selkoe, D. J. Alzheimer's disease: Genes, proteins, and therapy. *Physiol. Rev.* **2001,** *81*, 741–766.

(3) Selkoe, D. J. Imaging Alzheimer's amyloid. *Nat. Biotechnol.* **2000,** *18*, 823–824.

(4) Mathis, C. A.; Wang, Y.; Klunk, W. E. Imaging β-amyloid plaques and neurofibrillary tangles in the aging human brain. *Curr. Pharm. Des.* **2004,** *10*, 1469–1492.

(5) Nordberg, A. PET imaging of amyloid in Alzheimer's disease. *Lancet Neurol.* **2004,** *3*, 519–527.

(6) Kung, H. F.; Choi, S. R.; Qu, W.; Zhang, W.; Skovronsky, D. ^{18}F Stilbenes and Styrylpyridines for PET Imaging of Aβ Plaques in Alzheimer's Disease: A Miniperspective. *J. Med. Chem.* **2010,** *53*, 933–941.

(7) Mathis, C. A.; Wang, Y.; Holt, D. P.; Huang, G. F.; Debnath, M. L.; Klunk, W. E. Synthesis and evaluation of ^{11}C-labeled 6-substituted 2-arylbenzothiazoles as amyloid imaging agents. *J. Med. Chem.* **2003,** *46*, 2740–2754.

(8) Klunk, W. E.; Engler, H.; Nordberg, A.; Wang, Y.; Blomqvist, G.; Holt, D. P.; Bergstrom, M.; Savitcheva, I.; Huang, G. F.; Estrada, S.; Ausen, B.; Debnath, M. L.; Barletta, J.; Price, J. C.; Sandell, J.; Lopresti, B. J.; Wall, A.; Koivisto, P.; Antoni, G.; Mathis, C. A.; Langstrom, B. Imaging brain amyloid in Alzheimer's disease with Pittsburgh Compound-B. *Ann. Neurol.* **2004,** *55*, 306–319.

(9) Ono, M.; Wilson, A.; Nobrega, J.; Westaway, D.; Verhoeff, P.; Zhuang, Z. P.; Kung, M. P.; Kung, H. F. ^{11}C-labeled stilbene derivatives as Aβ-aggregate-specific PET imaging agents for Alzheimer's disease. *Nucl. Med. Biol.* **2003,** *30*, 565–571.

(10) Verhoeff, N. P.; Wilson, A. A.; Takeshita, S.; Trop, L.; Hussey, D.; Singh, K.; Kung, H. F.; Kung, M. P.; Houle, S. In-vivo imaging of Alzheimer disease β-amyloid with [^{11}C]SB-13 PET. *Am. J. Geriatr. Psychiatry* **2004,** *12*, 584–595.

(11) Zhang, W.; Oya, S.; Kung, M. P.; Hou, C.; Maier, D. L.; Kung, H. F. F-18 polyethyleneglycol stilbenes as PET imaging agents targeting Aβ aggregates in the brain. *Nucl. Med. Biol.* **2005,** *32*, 799–809.

(12) Rowe, C. C.; Ackerman, U.; Browne, W.; Mulligan, R.; Pike, K. L.; O'Keefe, G.; Tochon-Danguy, H.; Chan, G.; Berlangieri, S. U.; Jones, G.; Dickinson-Rowe, K. L.; Kung, H. P.; Zhang, W.; Kung, M. P.; Skovronsky, D.; Dyrks, T.; Holl, G.; Krause, S.; Friebe, M.; Lehman, L.; Lindemann, S.; Dinkelborg, L. M.; Masters, C. L.; Villemagne, V. L. Imaging of amyloid β in Alzheimer's disease with ^{18}F-BAY94-9172, a novel PET tracer: Proof of mechanism. *Lancet Neurol.* **2008,** *7*, 129–135.

(13) Kudo, Y.; Okamura, N.; Furumoto, S.; Tashiro, M.; Furukawa, K.; Maruyama, M.; Itoh, M.; Iwata, R.; Yanai, K.; Arai, H. 2-(2-[2-Dimethylaminothiazol-5-yl]ethenyl)-6-(2-[fluoro]ethoxy)-benzoxazole: A novel PET agent for in vivo detection of dense amyloid plaques in Alzheimer's disease patients. *J. Nucl. Med.* **2007,** *48*, 553–561.

(14) Agdeppa, E. D.; Kepe, V.; Liu, J.; Flores-Torres, S.; Satyamurthy, N.; Petric, A.; Cole, G. M.; Small, G. W.; Huang, S. C.; Barrio, J. R. Binding characteristics of radiofluorinated 6-dialkylamino-2-naphthylethylidene derivatives as positron emission tomography imaging probes for β-amyloid plaques in Alzheimer's disease. *J. Neurosci.* **2001,** *21*, RC189.

(15) Shoghi-Jadid, K.; Small, G. W.; Agdeppa, E. D.; Kepe, V.; Ercoli, L. M.; Siddarth, P.; Read, S.; Satyamurthy, N.; Petric, A.; Huang, S. C.; Barrio, J. R. Localization of neurofibrillary tangles and β-amyloid plaques in the brains of living patients with Alzheimer disease. *Am. J. Geriatr. Psychiatry* **2002,** *10*, 24–35.

(16) Small, G. W.; Kepe, V.; Ercoli, L. M.; Siddarth, P.; Bookheimer, S. Y.; Miller, K. J.; Lavretsky, H.; Burggren, A. C.; Cole, G. M.; Vinters, H. V.; Thompson, P. M.; Huang, S. C.; Satyamurthy, N.; Phelps, M. E.; Barrio, J. R. PET of brain amyloid and tau in mild cognitive impairment. *N. Engl. J. Med.* **2006,** *355*, 2652–2663.

(17) Kung, M. P.; Hou, C.; Zhuang, Z. P.; Zhang, B.; Skovronsky, D.; Trojanowski, J. Q.; Lee, V. M.; Kung, H. F. IMPY: An improved thioflavin-T derivative for *in vivo* labeling of β-amyloid plaques. *Brain Res.* **2002,** *956*, 202–210.

(18) Zhuang, Z. P.; Kung, M. P.; Wilson, A.; Lee, C. W.; Plossl, K.; Hou, C.; Holtzman, D. M.; Kung, H. F. Structure-activity relationship of imidazo[1,2-a]pyridines as ligands for detecting β-amyloid plaques in the brain. *J. Med. Chem.* **2003,** *46*, 237–243.

(19) Newberg, A. B.; Wintering, N. A.; Clark, C. M.; Plossl, K.; Skovronsky, D.; Seibyl, J. P.; Kung, M. P.; Kung, H. F. Use of ^{123}I IMPY SPECT to differentiate Alzheimer's disease from controls. *J. Nucl. Med.* **2006,** *47*, 78P.

(20) Zhang, W.; Kung, M. P.; Oya, S.; Hou, C.; Kung, H. F. ^{18}F-labeled styrylpyridines as PET agents for amyloid plaque imaging. *Nucl. Med. Biol.* **2007,** *34*, 89–97.

(21) Choi, S. R.; Golding, G.; Zhuang, Z.; Zhang, W.; Lim, N.; Hefti, F.; Benedum, T. E.; Kilbourn, M. R.; Skovronsky, D.; Kung, H. F. Preclinical properties of ^{18}F-AV-45: A PET agent for Aβ plaques in the brain. *J. Nucl. Med.* **2009,** *50*, 1887–1894.

(22) Ono, M.; Kung, M. P.; Hou, C.; Kung, H. F. Benzofuran derivatives as Aβ-aggregate-specific imaging agents for Alzheimer's disease. *Nucl. Med. Biol.* **2002,** *29*, 633–642.

(23) Ono, M.; Kawashima, H.; Nonaka, A.; Kawai, T.; Haratake, M.; Mori, H.; Kung, M. P.; Kung, H. F.; Saji, H.; Nakayama, M. Novel benzofuran derivatives for PET imaging of β-amyloid plaques in Alzheimer's disease brains. *J. Med. Chem.* **2006,** *49*, 2725–2730.

(24) Han, H.; Cho, C. G.; Lansbury, P. T., Jr. Technetium complexes for the quantitation of brain amyloid. *J. Am. Chem. Soc.* **1996,** *118*, 4506–4507.

(25) Dezutter, N. A.; Dom, R. J.; de Groot, T. J.; Bormans, G. M.; Verbruggen, A. M. ^{99m}Tc-MAMA-chrysamine G, a probe for β-amyloid protein of Alzheimer's disease. *Eur. J. Nucl. Med.* **1999,** *26*, 1392–1399.

(26) Chen, X.; Yu, P.; Zhang, L.; Liu, B. Synthesis and biological evaluation of ^{99m}Tc, Re-monoamine-monoamide conjugated to 2-(4-aminophenyl)benzothiazole as potential probes for β-amyloid plaques in the brain. *Bioorg. Med. Chem. Lett.* **2008,** *18*, 1442–1445.

(27) Serdons, K.; Verduyckt, T.; Cleynhens, J.; Terwinghe, C.; Mortelmans, L.; Bormans, G.; Verbruggen, A. Synthesis and evaluation of a ^{99m}Tc-BAT-phenylbenzothiazole conjugate as a potential in vivo tracer for visualization of amyloid β. *Bioorg. Med. Chem. Lett.* **2007,** *17*, 6086–6090.

(28) Zhuang, Z. P.; Kung, M. P.; Hou, C.; Ploessl, K.; Kung, H. F. Biphenyls labeled with technetium 99m for imaging β-amyloid plaques in the brain. *Nucl. Med. Biol.* **2005,** *32*, 171–184.

(29) Oya, S.; Plossl, K.; Kung, M. P.; Stevenson, D. A.; Kung, H. F. Small and neutral Tc(v)O BAT, bisaminoethanethiol (N_2S_2) complexes for developing new brain imaging agents. *Nucl. Med. Biol.* **1998,** *25*, 135–140.

DOI: 10.1021/ml100140d | *ACS Med. Chem. Lett.* **2010,** *1*, 443–447

Bioorganic & Medicinal Chemistry Letters 20 (2010) 6141–6144

Contents lists available at ScienceDirect

Bioorganic & Medicinal Chemistry Letters

journal homepage: www.elsevier.com/locate/bmcl

A novel ^{18}F-labeled pyridyl benzofuran derivative for imaging of β-amyloid plaques in Alzheimer's brains

Yan Cheng [a], Masahiro Ono [a,*], Hiroyuki Kimura [a], Shinya Kagawa [b], Ryuichi Nishii [b], Hideo Saji [a,*]

[a] Graduate School of Pharmaceutical Sciences, Kyoto University, 46-29 Yoshida Shimoadachi-cho, Sakyo-ku, Kyoto 606-8501, Japan
[b] Shiga Medical Center Research Institute, 5-4-30, Moriyama, Moriyama City, Shiga 524-8524, Japan

ARTICLE INFO

Article history:
Received 20 May 2010
Revised 22 July 2010
Accepted 4 August 2010
Available online 8 August 2010

Keywords:
Alzheimer's disease
β-Amyloid plaques
Positron emission tomography (PET)
Benzofuran

ABSTRACT

A potential probe for PET targeting β-amyloid plaques in Alzheimer's disease (AD) brain, FPYBF-1 (5-(5-(2-(2-(2-fluoroethoxy)ethoxy)ethoxy)benzofuran-2-yl)-*N*,*N*-dimethylpyridin-2-amine), was synthesized and evaluated. In experiments in vitro, FPYBF-1 displayed high affinity for Aβ(1–42) aggregates (K_i = 0.9 nM), and substantial labeling of β-amyloid plaques in sections of postmortem AD brains but not control brains. In experiments in vivo, [^{18}F]FPYBF-1 displayed good initial uptake (5.16%ID/g at 2 min postinjection) and rapid washout from the brain (2.44%ID/g at 60 min postinjection) in normal mice, and excellent binding to β-amyloid plaques in a murine model of AD. Furthermore, the specific labeling of plaques labeling was observed in autoradiographs of autopsied AD brain sections. [^{18}F]FPYBF-1 may be a useful probe for imaging β-amyloid plaques in living brain tissue.

Alzheimer's disease (AD) is a progressive neurodegenerative disorder characterized by cognitive decline, irreversible memory loss, disorientation, and language impairment. The presence of β-amyloid (Aβ) aggregates in the brain is generally accepted as a hallmark of AD.[1,2] Since the only definitive diagnosis of AD is by pathological examination of autopsied brain tissue, the development of techniques which enable the imaging of β-amyloid plaques in vivo has been strongly desired.[3–5]

Preliminary studies with positron emission tomography (PET) suggested that [^{11}C]4-*N*-methylamino-4′-hydroxystilbene (SB-13),[6,7] [^{11}C] 2-(4′-(methylaminophenyl)-6-hydroxybenzothiazole (PIB),[8,9] [^{11}C]2-(2-[2-dimethylaminothiazol-5-yl]ethenyl)-6-(2-[fluoro]ethoxy)benzoxazole (BF-227),[10] and [^{11}C]-2-[6-(methylamino)pyridin-3-yl]-1,3-benzothiazol-6-ol (AZD2184)[11] differed in their uptake and retention in the brain between AD patients and controls (Fig. 1). Success in using ^{11}C-labeled tracers to image β-amyloid plaques in the brain in cases of suspected AD has provided considerable impetus for further refinement of this technique. However, the short half-life of ^{11}C ($t_{1/2}$: 20 min) limits its potential as a diagnostic tool. Since ^{18}F with a longer half-life isotope ($t_{1/2}$: 110 min) would be more useful for this purpose, recent efforts have focused on the development of comparable agents labeled with ^{18}F. Preliminary studies with [^{18}F]-2-(1-(2-(*N*-(2-fluoroethyl)-*N*-methylamino)naphthalene-6-yl)ethylidene)malononitrile (FDDNP)[12,13] showed differential uptake and retention in the brain of AD patients for the first time. More recently, a stilbene derivative, (*E*)-4-(*N*-methylamino)-4′-(2-(2-(2-[^{18}F]-fluoroethoxy)ethoxy)-ethoxy)-stilbene (BAY94-9172),[14,15] a styryl pyridine derivative, (*E*)-4-(2-(6-(2-(2-(2-([^{18}F]-fluoroethoxy)ethoxy)ethoxy)pyridyn-3-ylvinyl)-*N*-methyl benzenamine (AV-45),[16–18] and a PIB analogue, 2-(3-[^{18}F]-fluoro-4-methyamino-phenyl)benzothiazol-6-ol (GE-067),[19] have been shown to be useful for the imaging of β-amyloid plaques in living brain tissue in phase II or III clinical trials (Fig. 1).[20]

We have evaluated a series of fluorinated benzofuran derivatives as potential ^{18}F-labeled tracers for the imaging of β-amyloid plaques by PET.[21] These derivatives displayed excellent affinity for Aβ aggregates in vitro and in vivo. The penetration of brain tissues by 4-(5-(2-(2-(2-fluoroethoxy)ethoxy)ethoxy)benzofuran-2-yl)-*N*,*N*-dimethylbenzenamine (FPHBF-1, Fig. 2) was particularly encouraging. However, the slow washout of this probe from the normal mouse brain made it unsuitable for imaging in vivo. Therefore, a critical need to fine-tune the kinetics of the uptake and washout of benzofuran derivatives exists. Previous results regarding uptake into and clearance from the brain point to high lipophilicity as one of the reasons for a slow washout from the brain.[8,22–24]

We planned to develop a novel fluorinated pyridyl benzofuran derivative with less lipophilicity by displacing of the phenyl group in phenyl benzofuran with a pyridyl group. Kung and co-workers exploited a novel approach, fluoro-pegylation (FPEG) of the core structure, to label derivatives with ^{18}F.[25] Since this approach offers

* Corresponding authors. Tel.: +81 75 753 4608; fax: +81 75 753 4568 (M.O.); tel.: +81 75 753 4556; fax: +81 75 753 4568 (H.S.).
E-mail addresses: ono@pharm.kyoto-u.ac.jp (M. Ono), hsaji@pharm.kyoto-u.ac.jp (H. Saji).

0960-894X/$ - see front matter © 2010 Elsevier Ltd. All rights reserved.
doi:10.1016/j.bmcl.2010.08.016

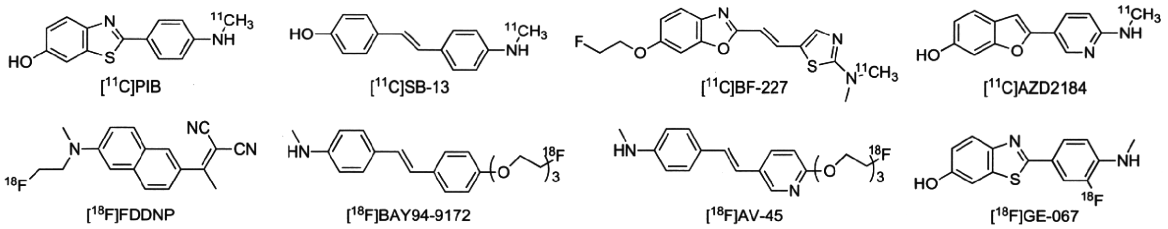

Figure 1. Chemical structure of PET imaging agents targeting β-amyloid plaques in AD patients.

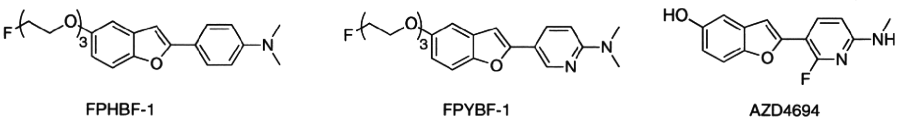

Figure 2. Chemical structure of benzofuran derivatives, FPHBF-1, FPYBF-1, and AZD4694.

a simple and easy way to incorporate ^{18}F into a target without an appreciable increase in lipophilicity, we selected FPEG for the labeling of pyridyl benzofuran derivatives. We designed a novel fluorinated ligand, 5-(5-(2-(2-(2-fluoroethoxy)ethoxy)ethoxy)benzofuran-2-yl)-*N*,*N*-dimethylpyridin-2-amine (FPYBF-1, Fig. 2) with a fluoropolyethylene glycol side chain and a dimethylamino pyridyl group. Another group recently reported a different fluorinated pyridyl benzofuran derivative, 2-(2-fluoro-6-(methylamino)pyridin-3-yl)benzofuran-5-ol (AZD4694, Fig. 2) to have potential for the imaging of cerebral β-amyloid plaques in living brain tissue.[26] However, they did not report the ^{18}F-labeling or in vivo characteristics of [^{18}F]AZD4694. This is the first time that a pyridyl benzofuran derivative has been successfully radiolabeled with ^{18}F and evaluated for the imaging of β-amyloid plaques in vivo.

The synthesis of **5** (FPYBF-1) is outlined in Scheme 1. The key step in the formation of the pyridyl benzofuran backbone is accomplished by Suzuki coupling between 5-methoxybenzofuran-2-boronic acid and 2-amino-5-iodopyridine.[27] Suzuki coupling afforded the desired compound **1** in a yield of 52.1%. Conversion of **1** to the corresponding dimethylamino derivative **2** was achieved by dimethylation with paraformaldehyde and sodium cyanoborohydride (yield 62%). A methoxy group of **2** was converted to a hydroxyl group using BBr_3/CH_2Cl_2, which afforded **3** in a yield of 98.9%. The synthesis of **4**–**6** was achieved using conventional methods reported previously.[28] The ^{18}F-labeled **5** ([^{18}F]FPYBF-1) was prepared from a tosyl precursor (**6**) via a nucleophilic displacement reaction with a fluoride anion as shown in Scheme 2. Radiolabeling of the precursor generated [^{18}F]FPYBF-1 with an average radiochemical yield of 52% and radiochemical purity of >99%, and a specific activity of 242 GBq/μmol. The identity of [^{18}F]FPYBF-1 was verified by a comparison of the retention time with the nonradioactive compound.

Experiments in vitro to evaluate the affinity of FPYBF-1 for Aβ aggregates were carried out in solutions with [^{125}I]IMPY as the ligand according to conventional methods.[29,30] FPYBF-1 inhibited the binding of [^{125}I]IMPY in a dose-dependent manner with a K_i value of 0.9 nM, indicating that it has excellent affinity for Aβ(1–42) aggregates (Fig. 3). This K_i value is similar to that of phenyl benzofuran derivatives (K_i = 2.0 nM) reported previously,[21] and the affinity of the pyridyl benzofuran derivative for Aβ(1–42) aggregates remained high despite displacement of the phenyl group with a pyridyl group. This result also shows that the benzofuran scaffold can tolerate extensive structural modification.[21,22,31]

To evaluate the uptake of [^{18}F]FPYBF-1 in the brain, a biodistribution experiment was performed in normal mice (Table 1).

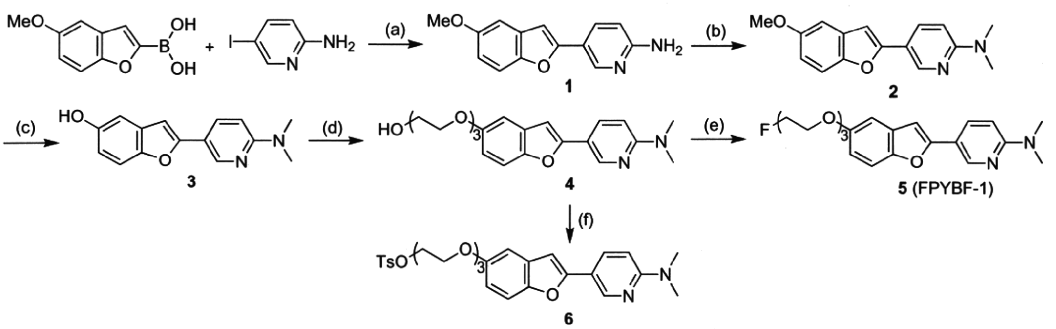

Scheme 1. Reagents and conditions: (a) $Pd(Ph_3P)_4$, Na_2CO_3 (aq)/dioxane, reflux.; (b) paraformaldehyde, sodium cyanoborohydride, acetic acid, rt; (c)BBr_3, CH_2Cl_2, rt; (d) 2-[2-(2-chloroethoxy)ethoxy]ethanol, K_2CO_3, DMF, 100 °C; (e) DAST, DME, 0 °C; (f) tosyl chloride, pyridine, rt.

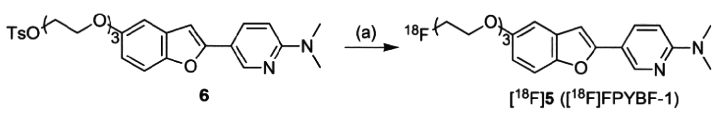

Scheme 2. Reagents and conditions: (a) Kryptofix222, K_2CO_3, acetonitrile, 120 °C.

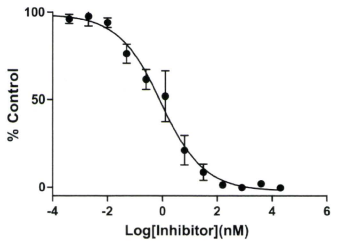

Figure 3. Competition curve of FPYBF-1 against [^{125}I]IMPY.

[^{18}F]FPYBF-1 displayed high uptake (5.16%ID/g) at 2 min postinjection, sufficient for PET, and the radioactivity in the brain cleared with time (2.44%ID/g at 60 min postinjection). Since normal brain tissue has no β-amyloid plaques to trap [^{18}F]FPYBF-1, the radioactivity should wash out quite rapidly. Therefore, the rapid clearance of [^{18}F]FPYBF-1 from normal brain is appropriate for the detection of β-amyloid plaques in the AD brain. One way to select a ligand with appropriate kinetics in vivo is to use the $brain_{2\ min}/brain_{60\ min}$ ratio as an index to compare the washout rate.[32] Although the $brain_{2\ min}/brain_{60\ min}$ ratio of [^{18}F]FPYBF-1 (2.1) was lower than that of [^{18}F]BAY94-9172 (4.8)[14] or [^{18}F]AV-45 (3.8),[16] it was improved as compared to the values for [^{18}F]FPHBF-1 (1.0) reported previously.[21] The favorable in vivo pharmacokinetics of [^{18}F]FPYBF-1 were achieved by changing the phenyl group in [^{18}F]FPHBF-1 to a pyridyl group. In HPLC analyses, [^{18}F]FPYBF-1 and [^{18}F]FPHBF-1 showed retention times of 14.8 and 36.5 min, respectively, indicating that [^{18}F]FPYBF-1 is less lipophilic than [^{18}F]FPHBF-1. Although lipophil-

Table 1
Biodistribution of radioactivity after injection of [^{18}F]FPYBF-1 in normal mice[a]

Organ	2 min	10 min	30 min	60 min
Blood	2.83 ± 0.89	2.13 ± 0.49	1.76 ± 0.09	1.98 ± 0.35
Brain	5.16 ± 0.30	3.75 ± 0.64	2.78 ± 0.22	2.44 ± 0.36
Bone	1.61 ± 0.33	1.33 ± 0.28	1.11 ± 0.13	1.42 ± 0.24

[a] Expressed as % of injected dose per gram. Each value represents the mean ± SD for five mice.

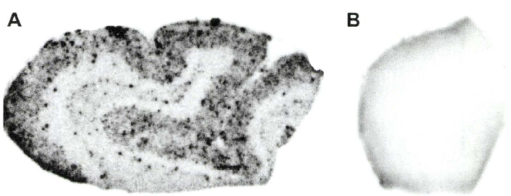

Figure 4. In vitro autoradiograms of sections of AD brain labeled with [^{18}F]FPYBF-1. Intensive labeling of β-amyloid plaques in brain tissue from AD patients (A). The control subject exhibits no labeling by this tracer (B).

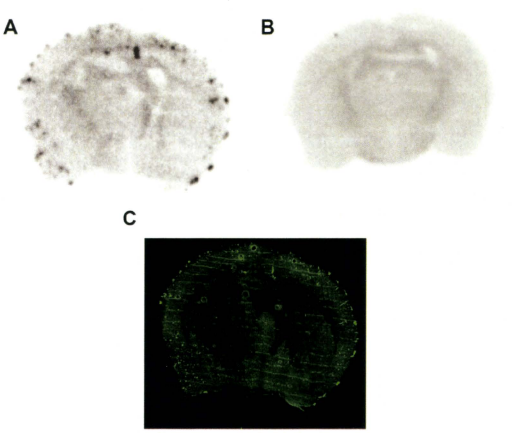

Figure 5. The labeling of β-amyloid plaques in vivo was visualized by autoradiography ex vivo with [^{18}F]FPYBF-1 in sections of Tg2576 mouse brain (A). The same section was also stained with thioflavin-S (C). Wild-type mouse brain showed no β-amyloid plaques (B).

icity is just one of the factors affecting the uptake of a compound into the brain,[4] it may explain the favorable pharmacokinetics of [^{18}F]FPYBF-1 in the brain. Uptake in the bone at 60 min was reduced (1.42%ID/g), suggesting little defluorination in vivo and interference with the imaging is expected to be relatively minor.

Next, sections of brain tissue from AD and control subjects (5 μm) were used to confirm the specific binding of [^{18}F]FPYBF-1 to β-amyloid plaques. Autoradiographic images revealed extensive labeling of β-amyloid plaques in the AD brain (Fig. 4A) but not control brain (Fig. 4B). The results suggest that [^{18}F]FPYBF-1 shows affinity for β-amyloid plaques in addition to synthetic Aβ aggregates.

To further characterize the potential of [^{18}F]FPYBF-1 as a probe for imaging β-amyloid plaques in living brain tissue, we carried out autoradiography ex vivo in Tg2576 mice (36 months, male) and in wild-type mice (36 months, male) as age-matched controls. Tg2576 transgenic mice show marked Aβ deposition in the cingulated cortex, entorhinal cortex, dentate gyrus, and CA1 hippocampal subfield by 11–13 months of age[33] and have been frequently used to evaluate the specific binding of β-amyloid plaques in experiments in vitro and in vivo.[28,34,35] The autoradiography showed clear labeling of β-amyloid plaques in the Tg2576 mouse brain (Fig. 5A). Wild-type mouse brain showed no such labeling (Fig. 5B). β-Amyloid plaques were confirmed present by co-staining the sections with thioflavin-S, a pathological dye commonly used to stain β-amyloid plaques (Fig. 5C). This is consistent with the results in vitro, showing [^{18}F]FPYBF-1 to be highly selective in binding to β-amyloid plaques in the brain.

In conclusion, based on previous results, we designed a novel fluorinated pyridyl benzofuran ligand, FPYBF-1, for the imaging of β-amyloid plaques in the brain. FPYBF-1 showed high binding affinity for Aβ aggregates in vitro and for β-amyloid plaques in sections of autopsied AD brain. It also displayed good uptake in the brain (5.16%ID/g at 2 min postinjection) and excellent binding to β-amyloid plaques ex vivo in transgenic mice. [^{18}F]FPYBF-1 is now under preclinical evaluation for use as a probe in PET. Other pyridyl benzofuran derivatives are also under investigation.

Acknowledgments

The study was supported by a Grant-in-aid for Young Scientists (A) and Exploratory Research from the Ministry of Education, Culture, Sports, Science and Technology.

Supplementary data

Supplementary data associated with this article can be found, in the online version, at doi:10.1016/j.bmcl.2010.08.016.

References and notes

1. Hardy, J. A.; Higgins, G. A. *Science* **1992**, *256*, 184.
2. Selkoe, D. J. *Physiol. Rev.* **2001**, *81*, 741.
3. Selkoe, D. J. *Nat. Biotechnol.* **2000**, *18*, 823.
4. Mathis, C. A.; Wang, Y.; Klunk, W. E. *Curr. Pharm. Des.* **2004**, *10*, 1469.
5. Nordberg, A. *Lancet Neurol.* **2004**, *3*, 519.
6. Ono, M.; Wilson, A.; Nobrega, J.; Westaway, D.; Verhoeff, P.; Zhuang, Z. P.; Kung, M. P.; Kung, H. F. *Nucl. Med. Biol.* **2003**, *30*, 565.
7. Verhoeff, N. P.; Wilson, A. A.; Takeshita, S.; Trop, L.; Hussey, D.; Singh, K.; Kung, H. F.; Kung, M. P.; Houle, S. *Am. J. Geriatr. Psychiatry* **2004**, *12*, 584.
8. Mathis, C. A.; Wang, Y.; Holt, D. P.; Huang, G. F.; Debnath, M. L.; Klunk, W. E. *J. Med. Chem.* **2003**, *46*, 2740.
9. Klunk, W. E.; Engler, H.; Nordberg, A.; Wang, Y.; Blomqvist, G.; Holt, D. P.; Bergstrom, M.; Savitcheva, I.; Huang, G. F.; Estrada, S.; Ausen, B.; Debnath, M. L.; Barletta, J.; Price, J. C.; Sandell, J.; Lopresti, B. J.; Wall, A.; Koivisto, P.; Antoni, G.; Mathis, C. A.; Langstrom, B. *Ann. Neurol.* **2004**, *55*, 306.
10. Kudo, Y.; Okamura, N.; Furumoto, S.; Tashiro, M.; Furukawa, K.; Maruyama, M.; Itoh, M.; Iwata, R.; Yanai, K.; Arai, H. *J. Nucl. Med.* **2007**, *48*, 553.
11. Johnson, A. E.; Jeppsson, F.; Sandell, J.; Wensbo, D.; Neelissen, J. A.; Jureus, A.; Strom, P.; Norman, H.; Farde, L.; Svensson, S. P. *J. Neurochem.* **2009**, *108*, 1177.
12. Agdeppa, E. D.; Kepe, V.; Liu, J.; Flores-Torres, S.; Satyamurthy, N.; Petric, A.; Cole, G. M.; Small, G. W.; Huang, S. C.; Barrio, J. R. *J. Neurosci.* **2001**, *21*, RC189.
13. Shoghi-Jadid, K.; Small, G. W.; Agdeppa, E. D.; Kepe, V.; Ercoli, L. M.; Siddarth, P.; Read, S.; Satyamurthy, N.; Petric, A.; Huang, S. C.; Barrio, J. R. *Am. J. Geriatr. Psychiatry* **2002**, *10*, 24.
14. Zhang, W.; Oya, S.; Kung, M. P.; Hou, C.; Maier, D. L.; Kung, H. F. *Nucl. Med. Biol.* **2005**, *32*, 799.
15. Rowe, C. C.; Ackerman, U.; Browne, W.; Mulligan, R.; Pike, K. L.; O'Keefe, G.; Tochon-Danguy, H.; Chan, G.; Berlangieri, S. U.; Jones, G.; Dickinson-Rowe, K. L.; Kung, H. P.; Zhang, W.; Kung, M. P.; Skovronsky, D.; Dyrks, T.; Holl, G.; Krause, S.; Friebe, M.; Lehman, L.; Lindemann, S.; Dinkelborg, L. M.; Masters, C. L.; Villemagne, V. L. *Lancet Neurol.* **2008**, *7*, 129.
16. Zhang, W.; Kung, M. P.; Oya, S.; Hou, C.; Kung, H. F. *Nucl. Med. Biol.* **2007**, *34*, 89.
17. Choi, S. R.; Golding, G.; Zhuang, Z.; Zhang, W.; Lim, N.; Hefti, F.; Benedum, T. E.; Kilbourn, M. R.; Skovronsky, D.; Kung, H. F. *J. Nucl. Med.* **2009**, *50*, 1887.
18. Wong, D. F.; Rosenberg, P. B.; Zhou, Y.; Kumar, A.; Raymont, V.; Ravert, H. T.; Dannals, R. F.; Nandi, A.; Brasic, J. R.; Ye, W.; Hilton, J.; Lyketsos, C.; Kung, H. F.; Joshi, A. D.; Skovronsky, D. M.; Pontecorvo, M. J. *J. Nucl. Med.* **2010**, *51*, 913.
19. Koole, M.; Lewis, D. M.; Buckley, C.; Nelissen, N.; Vandenbulcke, M.; Brooks, D. J.; Vandenberghe, R.; Van Laere, K. *J. Nucl. Med.* **2009**, *50*, 818.
20. Kung, H. F.; Choi, S. R.; Qu, W.; Zhang, W.; Skovronsky, D. *J. Med. Chem.* **2010**, *53*, 933.
21. Cheng, Y.; Ono, M.; Kimura, H.; Kagawa, S.; Nishii, R.; Kawashima, H.; Saji, H. *ACS Med. Chem. Lett.* in press, doi:10.1021/ml100082x.
22. Ono, M.; Kawashima, H.; Nonaka, A.; Kawai, T.; Haratake, M.; Mori, H.; Kung, M. P.; Kung, H. F.; Saji, H.; Nakayama, M. *J. Med. Chem.* **2006**, *49*, 2725.
23. Ono, M.; Yoshida, N.; Ishibashi, K.; Haratake, M.; Arano, Y.; Mori, H.; Nakayama, M. *J. Med. Chem.* **2005**, *48*, 7253.
24. Ono, M.; Haratake, M.; Mori, H.; Nakayama, M. *Bioorg. Med. Chem.* **2007**, *15*, 6802.
25. Stephenson, K. A.; Chandra, R.; Zhuang, Z. P.; Hou, C.; Oya, S.; Kung, M. P.; Kung, H. F. *Bioconjugate Chem.* **2007**, *18*, 238.
26. Jureus, A.; Swahn, B. M.; Sandell, J.; Jeppsson, F.; Johnson, A. E.; Johnstrom, P.; Neelissen, J. A.; Sunnemark, D.; Farde, L.; Svensson, S. P. *J. Neurochem.* **2010**.
27. Miyaura, N.; Yamada, K.; Suzuki, A. *Tetrahedron Lett.* **1979**, *36*, 3437.
28. Ono, M.; Watanabe, R.; Kawashima, H.; Cheng, Y.; Kimura, H.; Watanabe, H.; Haratake, M.; Saji, H.; Nakayama, M. *J. Med. Chem.* **2009**, *52*, 6394.
29. Ono, M.; Haratake, M.; Saji, H.; Nakayama, M. *Bioorg. Med. Chem.* **2008**, *16*, 6867.
30. Watanabe, H.; Ono, M.; Ikeoka, R.; Haratake, M.; Saji, H.; Nakayama, M. *Bioorg. Med. Chem.* **2009**, *17*, 6402.
31. Ono, M.; Kung, M. P.; Hou, C.; Kung, H. F. *Nucl. Med. Biol.* **2002**, *29*, 633.
32. Maya, Y.; Ono, M.; Watanabe, H.; Haratake, M.; Saji, H.; Nakayama, M. *Bioconjugate Chem.* **2009**, *20*, 95.
33. Hsiao, K.; Chapman, P.; Nilsen, S.; Eckman, C.; Harigaya, Y.; Younkin, S.; Yang, F.; Cole, G. *Science* **1996**, *274*, 99.
34. Ono, M.; Hayashi, S.; Kimura, H.; Kawashima, H.; Nakayama, M.; Saji, H. *Bioorg. Med. Chem.* **2009**, *17*, 7002.
35. Ono, M.; Watanabe, R.; Kawashima, H.; Kawai, T.; Watanabe, H.; Haratake, M.; Saji, H.; Nakayama, M. *Bioorg. Med. Chem.* **2009**, *17*, 2069.

Tissue Factor Detection for Selectively Discriminating Unstable Plaques in an Atherosclerotic Rabbit Model

Takashi Temma[1], Yuki Ogawa[1], Yuji Kuge[1,2], Seigo Ishino[1], Nozomi Takai[1], Kantaro Nishigori[1], Masashi Shiomi[3], Masahiro Ono[1], and Hideo Saji[1]

[1]Department of Patho-Functional Bioanalysis, Graduate School of Pharmaceutical Sciences, Kyoto University, Sakyo-ku, Kyoto, Japan; [2]Central Institute of Isotope Science, Hokkaido University, Kita-ku, Sapporo, Japan; and [3]Institute for Experimental Animals, Kobe University Graduate School of Medicine, Chuo-ku, Kobe, Japan

Tissue factor (TF), a transmembrane glycoprotein that acts as an essential cofactor to factor VII/VIIa, initiates the exogenous blood coagulation cascade leading to thrombin generation and subsequent thrombus formation in vivo. TF expression is closely related to plaque vulnerability, and high TF expression is shown in macrophage-rich atheromatous lesions, making TF a potential target for detecting atheromatous lesions in vivo. Thus, we prepared ^{99m}Tc-labeled anti-TF-monoclonal antibody (TF-mAb) IgG as a molecular probe and evaluated its usefulness to achieve TF-specific imaging using myocardial infarction–prone Watanabe heritable hyperlipidemic (WHHLMI) rabbits. **Methods:** Anti-TF-mAb was created using a standard hybridoma technique and was labeled by ^{99m}Tc with 6-hydrazinonicotinic acid (HYNIC) as a chelating agent to obtain ^{99m}Tc-TF-mAb. The immunoreactivity of HYNIC-TF-mAb was estimated by flow cytometry. WHHLMI and control rabbits were injected intravenously with ^{99m}Tc-TF-mAb. Twenty-four hours after the injection, the aorta was removed and radioactivity was measured. Autoradiography and histologic studies were performed using serial aorta sections. Subclass matched antibody (IgG_1) was used as a negative control. **Results:** HYNIC-TF-mAb showed 93% immunoreactivity of the anti-TF-mAb. The radioactivity accumulation in WHHLMI aortas was 6.1-fold higher than that of control rabbits. Autoradiograms showed a heterogeneous distribution of radioactivity in the intima of WHHLMI aortas. Regional radioactivity accumulation was positively correlated with TF expression density ($R = 0.64$, $P < 0.0001$). The highest radioactivity accumulation in percentage injected dose × body weight/mm^2 × 10^2 was found in atheromatous lesions (5.2 ± 1.9) followed by fibroatheromatous (2.1 ± 0.7), collagen-rich (1.8 ± 0.7), and neointimal lesions (1.8 ± 0.6). In contrast, ^{99m}Tc-IgG_1 showed low radioactivity accumulation in WHHLMI aortas that was independent of the histologic grade of lesions. **Conclusion:** The TF-detecting ability and preferential accumulation in atheromatous lesions of ^{99m}Tc-TF-mAb were demonstrated, indicating its potential for selective imaging of macrophage-rich atheromatous lesions in vivo.

Received Jul. 13, 2010; revision accepted Sep. 8, 2010.

For correspondence or reprints contact: Yuji Kuge, Central Institute of Isotope Science, Hokkaido University, Kita 15 Nishi 7, Kita-ku, Sapporo 060-8638, Japan.

E-mail: kuge@ric.hokudai.ac.jp

Key Words: tissue factor; radioimmunodetection; thrombus; atherosclerotic plaque

J Nucl Med 2010; 51:1979–1986

DOI: 10.2967/jnumed.110.081216

Thrombus formation triggered by plaque rupture is the most important mechanism leading to the onset of acute arterial disease and ischemic sudden death. Thus, the development of a method for detecting thrombus-forming vulnerable plaques before rupture has been clinically desired to more precisely estimate risk and provide effective treatment. Although several molecular imaging probes have been investigated (*1*,*2*), the target molecules of such probes were not directly related to the thrombotic process.

Tissue factor (TF), a transmembrane glycoprotein that acts as an essential cofactor to factor (F) VII/VIIa, initiates the exogenous blood coagulation cascade leading to thrombin generation and subsequent thrombus formation. TF expression was identified in atherosclerotic lesions, including in endothelial cells, smooth muscle cells, monocytes, and, especially, macrophages or foam cells (*3*). In human pathologic lesions, the TF content of de novo lipid-rich plaques was higher than that of stenotic fibrous plaques (*4*), and such lipid-rich plaque tissue was 6 times more thrombogenic than fibrous plaques. In addition, our recent study also demonstrated that TF expression was closely related to plaque vulnerability, with high TF expression specifically in macrophage-rich atheromatous lesions among heterogeneous atherosclerotic lesions (*5*). Given these data, TF is a potential target for probes detecting atheromatous lesions at higher risk for rupture in vivo.

In the present study, we prepared a monoclonal antibody to TF (TF-mAb) and labeled it with ^{99m}Tc (^{99m}Tc-TF-mAb) as a molecular probe. Using an atherosclerosis model (myocardial infarction–prone Watanabe heritable hyperlipidemic [WHHLMI] rabbits) (*6*), we investigated the accumulation of ^{99m}Tc-TF-mAb in atherosclerotic lesions in comparison with histologic characteristics and evaluated the potential of ^{99m}Tc-TF-mAb as a molecular probe for detecting vulnerable atheromatous lesions.

MATERIALS AND METHODS

Design and Preparation of ^{99m}Tc-TF-mAb and ^{99m}Tc-IgG$_1$

A monoclonal antibody (mouse IgG$_1$ subclass) for rabbit TF (193Ser-207Cys, extracellular domain) was established using a standard hybridoma technique. ^{99m}Tc-pertechnetate was eluted in saline solution on a daily basis from ^{99}Mo–^{99m}Tc generators (Ultra-Techne Kow; FUJIFILM RI Pharma Co., Ltd.).

Anti-TF-mAb was radiolabeled with ^{99m}Tc (^{99m}Tc-TF-mAb) after derivatization with 6-hydrazinonicotinic acid (HYNIC) (*7*), as previously reported (*8*). In brief, HYNIC-*N*-hydroxysuccinimide was reacted with TF-mAb, and the mixture was purified by size-exclusion filtration with a diafiltration membrane (Amicon Ultra 4 [molecular weight cutoff, 30,000]; Millipore Co.). An equal volume of ^{99m}Tc-(tricine)$_2$, prepared by the method of Larsen et al. (*9*), was added to the purified solution of HYNIC-TF-mAb to obtain ^{99m}Tc-TF-mAb. After purification by size-exclusion filtration with a PD-10 column, the radiochemical purity of ^{99m}Tc-TF-mAb was more than 95% by another size-exclusion filtration.

For the control study, negative control mouse IgG$_1$ (0102-01; Southern Biotechnology Associates Inc.) was used for the preparation of ^{99m}Tc-IgG$_1$. The radiochemical purity of ^{99m}Tc-IgG$_1$ was also estimated to be more than 95%.

Animals

All animal procedures were approved by the Kyoto University Animal Care Committee. Three male Japanese White rabbits (age, 3 mo) were used to obtain peritoneal macrophages. For biodistribution studies of ^{99m}Tc-TF-mAb, 5 WHHLMI rabbits (4 male, 1 female; age, 12–18 mo; mean weight ± SD, 3.4 ± 0.2 kg; supplied by the Institute for Experimental Animals, Kobe University School of Medicine, Japan) were used. Four male Japanese White rabbits (age, 3 mo; mean weight ± SD, 1.9 ± 0.2 kg) were used for the control study. For ^{99m}Tc-IgG$_1$ studies, 3 WHHLMI rabbits (1 male and 2 female; age, 11–12 mo; mean weight ± SD, 3.2 ± 0.1 kg) were used. The animals were fed standard chow and given water ad libitum.

Immunoreactivity of HYNIC-TF-mAb

Rabbit peritoneal macrophages were obtained by the method of Ishii et al. (*10*), with minor modifications. Cells were suspended at a final concentration of 2.5×10^6 cells/mL in medium A (Dulbecco's modified Eagle's medium containing 1 mM glutamine, 100 U of penicillin per milliliter, 100 mg of streptomycin per milliliter [pH 7.4], and 0.2% lactalbumin hydrolysate). Aliquots of the cell suspension were cultured in plastic petri dishes in a humidified 5% CO_2 incubator at 37°C. After 2 h, each dish was washed twice with 10 mL of medium A to remove nonadherent cells. Monolayers were cultured for 18 h at 37°C in 20 mL of medium A, and cells were washed twice with 10 mL of medium A and then used for experiments. More than 95% of the cells were viable, as determined by a trypan blue exclusion test, and almost all of the attached cells showed positive nonspecific esterase staining.

Antibodies (5 μg/mL, 100 μL; TF-mAb, HYNIC-TF-mAb, or negative control IgG$_1$) were added to the cells (10^6) and incubated for 30 min at 4°C. After cells were washed, Alexa Fluor 488 goat antimouse IgG antibody (x0931; DakoCytomation) (10 μg/mL, 100 μL) was added for 30 min at 4°C. Fluorescence levels were measured using a flow cytometer (Becton Dickinson Inc.). Data were analyzed using BD CellQuest Pro (BD Biosciences), and an immunoreactivity index was calculated as the ratio of the median fluorescence intensity for either TF-mAb or HYNIC-TF-mAb to that of negative-control IgG$_1$. Measurements were performed 3 times per rabbit using 3 Japanese White rabbits, and the ratios were expressed as mean ± SD.

Biodistribution Studies

A simple schematic of our experimental protocol is shown in Figure 1. After 12 h of fasting, rabbits were initially anesthetized with ketamine (intramuscularly, 35 mg/kg) and xylazine (intramuscularly, 5 mg/kg). Either ^{99m}Tc-TF-mAb (547–1,024 MBq,

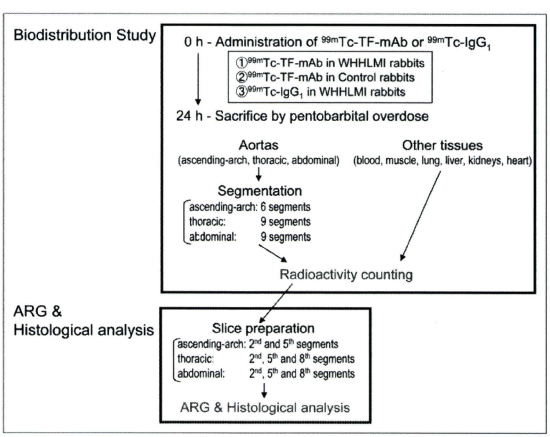

FIGURE 1. Simple schematic of this study. ARG = autoradiography.

300 μg) or ^{99m}Tc-IgG$_1$ (848–1,038 MBq, 300 μg) was injected into a marginal ear vein (5 WHHLMI rabbits and 4 control rabbits for the ^{99m}Tc-TF-mAb study, 3 WHHLMI rabbits for the ^{99m}Tc-IgG$_1$ study). Twenty-four hours after the injection, animals were sacrificed by pentobarbital overdose. The ascending-arch, thoracic, and abdominal aortas, blood, and other tissues (muscle, lung, liver, kidneys, and heart) were removed. The ascending-arch aortas were divided into 6 segments, and the thoracic and abdominal aortas were divided into 9 segments. Each segment was weighed and immediately fixed in a solution containing L-(+)-lysine hydrochloride (75 mM) and 4% paraformaldehyde in phosphate buffer (37.5 mM, pH 7.4) (*11*). The radioactivity of each sample was measured with a well-type γ-counter (1480 Wizard 3″; PerkinElmer Japan Co.). The results were expressed as the differential uptake ratio (DUR), calculated as (tissue activity/tissue weight)/(injected radiotracer activity/animal body weight), with activities given in becquerels and weights in grams. The aorta-to-blood (A/B) ratio and the aorta-to-muscle (A/M) ratio were calculated from the DUR for each tissue sample.

Autoradiography

Eight segments, the second and fifth segments of the ascending aortic arch and the second, fifth, and eighth segments from the thoracic and the abdominal aortas, from each animal were used for autoradiography studies. These segments were frozen and cut into 20-μm-thick slices with a cryomicrotome. The sections were thawed and mounted on silane-coated slides, which were then placed on a phosphor image plate (Fuji Imaging Plate BAS-MS; Fuji Photo Film) for 24 h together with a calibrated standard ($^{99m}TcO_4^-$ solution). The autoradiography images were analyzed with a computerized imaging analysis system (Bio Imaging Analyzer BAS2500 and Image Gauge Software; Fuji Photo Film). The radioactivity in each region of interest was expressed as percentage injected dose × body weight/mm^2, calculated as (radioactivity in the region of interest)/(injected radioactivity/animal body weight).

Histologic Analysis

The tissue sections used for autoradiography studies were also subjected to Azan–Mallory and hematoxylin and eosin staining. Serial sections of the slices from the autoradiography studies were subjected to immunohistochemical staining (for TF, macrophages, and smooth muscle cells) using specific antibodies and an Envision+ kit (Dako) with hematoxylin counterstaining. The antibodies used were TF-mAb (4510; American Diagnostica Inc.), rabbit macrophage–specific mAb RAM-11 (Dako), and human smooth-muscle actin–specific mAb 1A4 (Dako). Immunostaining with subclass-matched irrelevant IgG served as a negative control. Azan–Mallory and hematoxylin and eosin staining were performed by standard procedures. TF expression density was determined as a percentage of the positively stained region using a VHX digital microscope (Keyence Corp.).

Classification of Atherosclerotic Lesions

We divided atherosclerotic lesions in WHHLMI rabbits into the following 4 categories, using a classification scheme based on the recommendations of the American Heart Association (*12,13*) and Azan–Mallory and hematoxylin and eosin staining, as previously described (*14–17*): neointimal (types I–III), atheromatous (type IV), fibroatheromatous (types Va and Vb), and collagen-rich (type Vc). Supplemental Figures 1A–1P (supplemental materials are available online only at http://jnm.snmjournals.org) show representative photomicrographs of the histologic features of each atherosclerotic lesion category in WHHLMI rabbits.

Regions of interest were placed to cover each atherosclerotic lesion in the aortic section of the WHHLMI rabbit and then transferred to the corresponding autoradiography images (Supplemental Figs. 1Q–1S).

Vulnerability Index

An index of morphologic destabilization characteristics, the vulnerability index, was calculated for each lesion in the WHHLMI rabbits by the method of Shiomi et al. (*18*). The vulnerability index was defined as the ratio of the lipid component area (macrophages and extracellular lipid deposits) to the fibromuscular component area (smooth muscle cells and collagen fibers). Collagen fibers and extracellular lipid deposits (extracellular vacuoles and lacunae) were determined with Azan–Mallory stain-

TABLE 1
Accumulation Levels of ^{99m}Tc-TF-mAb and ^{99m}Tc-IgG$_1$ in Aortic Segments of Control and WHHLMI Rabbits at 24 Hours After Injection

Segments	^{99m}Tc-TF-mAb		^{99m}Tc-IgG$_1$, WHHLMI
	Control	WHHLMI	
Ascending arch	0.60 ± 0.05	3.08 ± 0.57*†	2.05 ± 0.42*
Thoracic	0.51 ± 0.11	3.07 ± 1.44*‡	1.60 ± 0.44*
Abdominal	0.35 ± 0.06	2.49 ± 0.64*‡	0.76 ± 0.16*
Total	0.47 ± 0.04	2.86 ± 0.85*‡	1.40 ± 0.24*
Blood	4.0 ± 0.6	7.5 ± 0.0*	7.1 ± 0.7§
Femoral muscle	0.6 ± 0.5	0.3 ± 0.2	0.4 ± 0.1
Aorta-to-blood ratio	0.12 ± 0.02	0.38 ± 0.09*‡	0.20 ± 0.02*
Aorta-to-muscle ratio	1.0 ± 0.6	19.3 ± 19.1*‡	4.0 ± 0.4*

*$P < 0.0001$ vs. control rabbits in ^{99m}Tc-TF-mAb study.
†$P < 0.001$ vs. WHHLMI rabbits in ^{99m}Tc-IgG$_1$ study.
‡$P < 0.0001$ vs. WHHLMI rabbits in ^{99m}Tc-IgG$_1$ study.
§$P < 0.001$, vs. control rabbits in ^{99m}Tc-TF-mAb study.
Data are represented as mean ± SD of DUR.

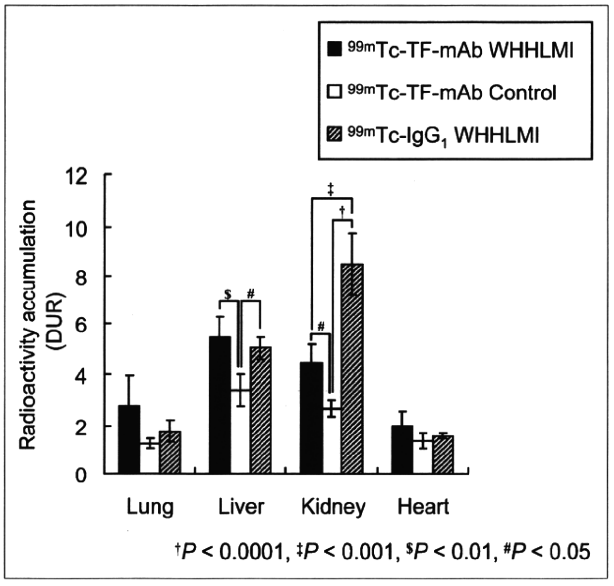

FIGURE 2. Radioactivity distribution in lung, liver, kidneys, and heart. Data are mean ± SD. †$P < 0.0001$. ‡$P < 0.001$. $$P < 0.01$. #$P < 0.05$.

ing. Macrophages and smooth muscle cells were determined with immunohistochemical staining (*17*).

Statistical Analysis

Data are presented as mean ± SD. Statistical analysis was performed with the Mann–Whitney *U* test to compare aortic segments of WHHLMI and control rabbits (Table 1). Radioactivity that accumulated in nontargeted organs among antibodies and animals was compared using 1-way ANOVA, with post hoc analysis by the Holm test (Fig. 2). Correlation coefficients were assessed by Spearman rank correlation coefficients (Fig. 3). Lesion types were compared using the Kruskal–Wallis test, with post hoc analysis by the Scheffé test (Fig. 4). A 2-tailed value of *P* less than 0.05 was considered statistically significant.

RESULTS

Immunoreactivity of HYNIC-TF-mAb

Using fluorescent-activated cell sorter analysis of rabbit peritoneal macrophages, we could clearly distinguish the signals of TF-mAb and HYNIC-TF-mAb from that of the negative control IgG_1. The median fluorescence intensity ratios of TF-mAb and HYNIC-TF-mAb to control IgG_1 were 2.90 ± 0.06 and 2.69 ± 0.11, respectively, and the difference between the labeled and unlabeled TF antibodies was not statistically significant.

Biodistribution Studies

Accumulation levels of ^{99m}Tc-TF-mAb and ^{99m}Tc-IgG_1 in the aortic segments of WHHLMI and control rabbits are summarized in Table 1. The accumulation level of ^{99m}Tc-TF-mAb in each aortic segment of WHHLMI rabbits (ascending arch, 3.08 ± 0.57 DUR; thoracic, 3.07 ± 1.44 DUR; and abdominal, 2.49 ± 0.64 DUR) was 5.1- to 7.1-fold higher than that of control rabbits (ascending arch, 0.60 ± 0.05 DUR; thoracic, 0.51 ± 0.11 DUR; and abdominal, 0.35 ± 0.06 DUR), and the differences were significant in each case. Blood-pool radioactivity levels of ^{99m}Tc-TF-mAb at 24 h were 7.5 ± 0.0 and 4.0 ± 0.6 DUR in WHHLMI and control rabbits, respectively. A/B and A/M ratios were significantly higher in WHHLMI rabbits than in control rabbits (A/B, 0.38 ± 0.09 in WHHLMI and 0.12 ± 0.02 in control rabbits; A/M, 19.3 ± 19.1 in WHHLMI and 1.0 ± 0.6 in control rabbits). In addition, the level of ^{99m}Tc-TF-mAb accumulation in WHHLMI rabbit aortas was 1.5- to 3.3-fold higher than the level of ^{99m}Tc-IgG_1 accumulation, and the differences were significant.

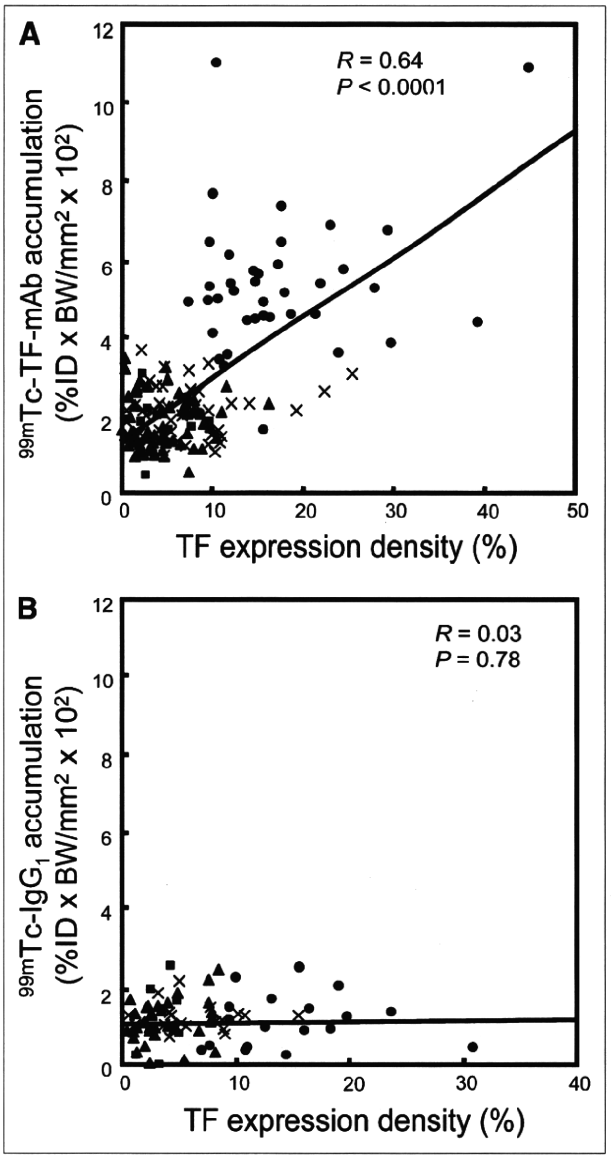

FIGURE 3. Regression analyses of TF expression density with ^{99m}Tc-TF-mAb (A) and ^{99m}Tc-IgG_1 (B) accumulation. ■ = neointimal lesion; ● = atheromatous lesion; × = fibroatheromatous lesion; ▲ = collagen-rich lesion.

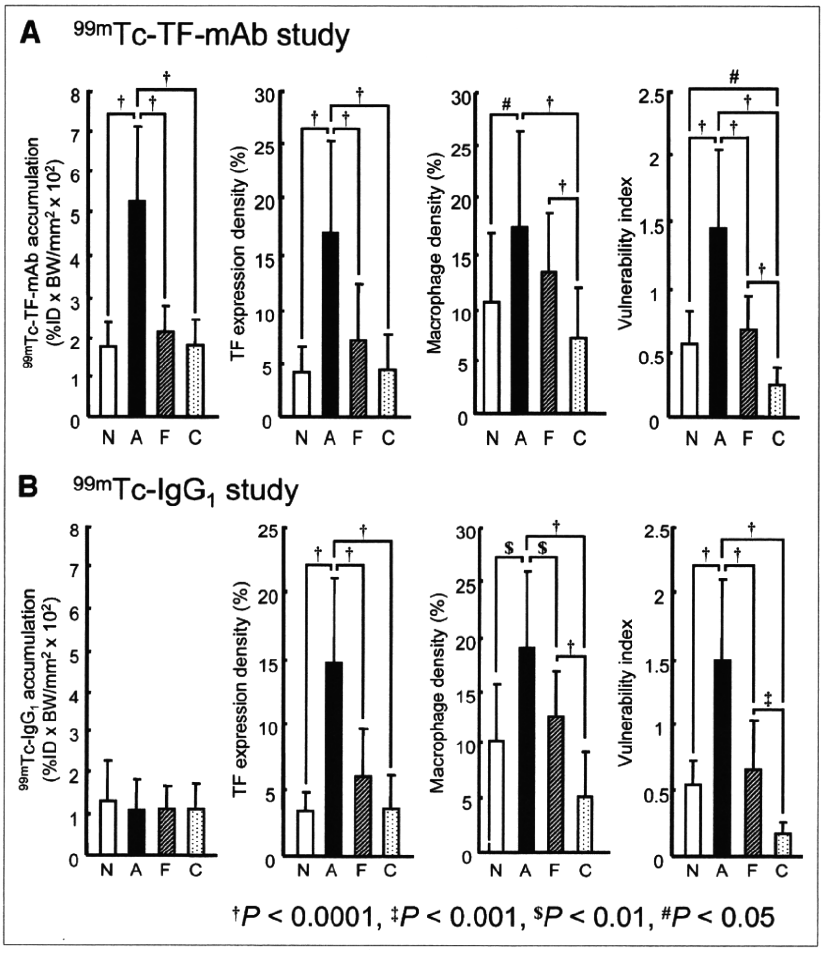

FIGURE 4. Distribution profiles of radioactivity accumulation, TF expression, macrophage density, and vulnerability index in atherosclerotic lesions in ^{99m}Tc-TF-mAb (A) and ^{99m}Tc-IgG$_1$ (B) study. A = atheromatous lesions; C = collagen-rich lesions; F = fibroatheromatous lesions; N = neointimal lesions. Data are represented as mean ± SD.

Relatively high radioactivity accumulations were found in the liver and kidneys of all 3 groups (Fig. 2). We observed that the ^{99m}Tc-TF-mAb cleared rather more slowly from the bodies of WHHLMI rabbits than from control rabbits.

Regional Distribution of ^{99m}Tc-TF-mAb, in Comparison with TF Expression

In the autoradiography study, heterogeneous ^{99m}Tc-TF-mAb accumulation was observed in the intima of WHHLMI rabbit aortas (Fig. 5B), whereas no marked accumulation was found in the aortas of control rabbits (Fig. 5A). Variable TF expression was detected in the intimal regions of the WHHLMI rabbit aorta (Figs. 5D, 5F, and 5G). Higher accumulation levels of ^{99m}Tc-TF-mAb were found in regions with high TF expression, whereas lower accumulation was observed in regions with low TF expression (Fig. 5, compare 5B with 5F and 5G). Consequently, regional ^{99m}Tc-TF-mAb accumulation levels in the aorta section were positively correlated with TF expression density in WHHLMI rabbits ($R = 0.64$, $P < 0.0001$) (Fig. 3A). No obvious TF expression was observed in the aorta of control rabbits (Figs. 5C, 5E, and 3B).

Relationship Between ^{99m}Tc-TF-mAb Accumulation and Histologic Characteristics

The plaques were categorized according to histopathologic classification criteria as follows: neointimal ($n = 12$ for ^{99m}Tc-TF-mAb study and $n = 7$ for ^{99m}Tc-IgG$_1$ study), atheromatous ($n = 40$ for ^{99m}Tc-TF-mAb study and $n = 20$ for ^{99m}Tc-IgG$_1$ study), fibroatheromatous ($n = 43$ for ^{99m}Tc-TF-mAb study and $n = 21$ for ^{99m}Tc-IgG$_1$ study), and collagen-rich ($n = 62$ for ^{99m}Tc-TF-mAb study and $n = 36$ for ^{99m}Tc-IgG$_1$ study). No lesions showed hemorrhage, plaque rupture, or thrombi (type VI). The level of ^{99m}Tc-TF-mAb accumulation was dependent on the histologic grade of the lesions (Fig. 4A) and was prominently and significantly the highest ($P < 0.0001$) in atheromatous lesions (type IV), compared with other lesions. The accumulation level of ^{99m}Tc-TF-mAb was 3.0-, 2.4-, and 2.9-fold higher in atheromatous lesions than in neointimal, fibroatheromatous, and collagen-rich lesions, respectively. The vulnerability index was also the highest in atheromatous lesions, followed in decreasing order by fibroatheromatous, neointimal, and collagen-rich lesions. Consequently, the highest level of ^{99m}Tc-TF-mAb accumulation and the highest vulnerability